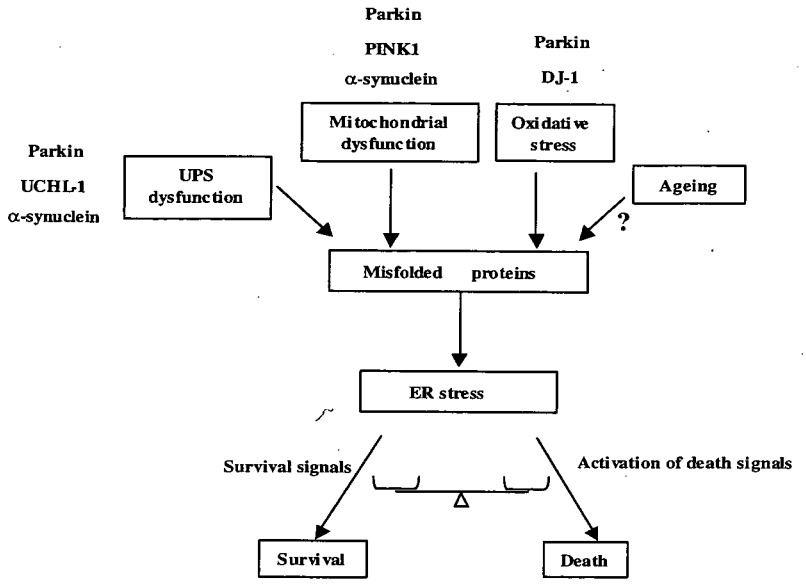

FIG. 6. Widespread involvement of ER stress in the pathogenesis of Parkinson's disease. In Parkinson's disease, proteasome dysfunction, oxidative stress, mitochondrial dysfunction, and possibly aging could directly or indirectly cause accumulation of misfolded proteins in the ER, thus induce ER stress. Cells counteract ER stress by activation of unfolded protein responses (UPR), which activates protective signals to eliminate misfolded proteins. However, when UPR fails to eliminate misfolded proteins, cells undergo apoptosis.

mechanism, whereby ER stress can result in secondary oxidative damage. One target of CHOP is ER oxidoreductase ERO1α, which participates in protein disulfide bond formation during protein refolding in the ER to help relieve ER stress, but in doing so also promotes production of ROS (28). The interplay between ER stress and oxidative stress might be mediated in part by parkin. Parkin is itself sensitive to oxidative stress, and is inactivated by nitric oxide-mediated nitrosylation or dopamine, which could lead to a simultaneous ER stress and oxidative damage (9, 24, 56). Inactivation of parkin is likely to create a feed-forward amplification loop, rendering dopaminergic cells more susceptible to oxidative and ER stress.

CONCLUSIONS

Evidence has been presented in various experimental studies that impairment of ER function may be involved in the neuronal cell death in PD. Environmental toxins, oxidative damage by dopamine itself, and mitochondrial abnormalities are all believed to play a role in sporadic PD (30). All these affect protein folding in the cytoplasm and lead to ER stress by compromising the process of ERAD (4). Alternatively, a genetic defect such as parkin mutation could impair the ability of cells to adapt to ER stress through impairment of its E3 activity. Since some novel components of the canonical UPR are expressed in a cell type-specific fashion, different types of cells may have unique responses for adaptation to ER stress (22, 32, 57). It is noted that parkin is upregulated in astrocytes, but not in neurons upon ER stress (25), suggesting parkin may represent as another unique response for adaptation to ER stress. Further investigation of parkin regulators will improve our chances of identifying novel targets for designing effective therapeutic strategies to impede the pathological processes.

ABBREVIATIONS

AD, Alzheimer's disease; ALS, amyotrophic lateral sclerosis; AR-JP, autosomal recessive juvenile Parkinsonism; bZIP, basic leucine zipper; CHIP, C-terminus of Hsc70 interaction protein; CHOP, C/EBP homologous protein; E2, ubiquitin conjugating enzyme; E3, ubiquitin ligase; eIF2α, eukaryotic initiation factor 2α; ER, endoplasmic reticulum; ERAD, ER-associated degradation; ERO1α, ER oxidoreductase 1α; GRP78, glucose regulated protein 78; Hsp70, heat shock protein 70; IBR, in-between RING; JNK, c-Jun NH2-terminal kinase; Pael-R, parkin associated endothelin like-receptor; ORP150, oxygen regulated protein 150; PINK1, PTEN-induced kinase 1; PD, Parkinson's disease; RING, really interesting new gene; ROS, reactive oxygen species; SNpc, substantia nigra pars compacta; TH, tyrosine hydroxylase; UPR, unfolded protein response; UPS, ubiquitin–proteasome system.

REFERENCES

1. Auluck PK, Chan HY, Trojanowski JQ, Lee VM, and Bonini NM. Chaperone suppression of alpha-synuclein toxicity in a *Drosophila* model for Parkinson's disease. *Science* 295: 865–868, 2002.
2. Back SH, Schroder M, Lee K, Zhang K, and Kaufman RJ. ER stress signaling by regulated splicing: IRE1/HAC1/XBP1. *Methods* 35: 395–416, 2005.
3. Beilina A, Van Der Brug M, Ahmad R, Kesavapany S, Miller DW, Petsko GA, and Cookson MR. Mutations in PTEN-induced putative kinase 1 associated with recessive parkinsonism have differential effects on protein stability. *Proc Natl Acad Sci USA* 102: 5703–5708, 2005.
4. Bence NF, Sampat RM, and Kopito RR. Impairment of the ubiquitin-proteasome system by protein aggregation. *Science* 292: 1552–1555, 2001.
5. Bertolotti A, Zhang Y, Hendershot LM, Harding HP, and Ron D. Dynamic interaction of BiP and ER stress transducers in the unfolded-protein response. *Nat Cell Biol* 2: 326–332, 2000.

6. Bonifati V, Rizzu P, van Baren MJ, Schaap O, Breedveld GJ, Krieger E, Dekker MC, Squitieri F, Ibanez P, Joosse M, van Dongen JW, Vanacore N, van Swieten JC, Brice A, Meco G, van Duijn CM, Oostra BA, and Heutink P. Mutations in the DJ-1 gene associated with autosomal recessive early-onset parkinsonism. *Science* 299: 256–259, 2003.
7. Braak H, Del Tredici K, Rub U, de Vos RA, Jansen Steur EN, and Braak E. Staging of brain pathology related to sporadic Parkinson's disease. *Neurobiol Aging* 24: 197–211, 2003.
8. Canet-Aviles RM, Wilson MA, Miller DW, Ahmad R, McLendon C, Bandyopadhyay S, Baptista MJ, Ringe D, Petsko GA, and Cookson MR. The Parkinson's disease protein DJ-1 is neuroprotective due to cysteine-sulfinic acid-driven mitochondrial localization. *Proc Natl Acad Sci USA* 101: 9103–9108, 2004.
9. Chung KK, Thomas B, Li X, Pletnikova O, Troncoso JC, Marsh L, Dawson VL, and Dawson TM. S-nitrosylation of parkin regulates ubiquitination and compromises parkin's protective function. *Science* 304: 1328–1331, 2004.
10. Cuervo AM, Stefanis L, Fredenburg R, Lansbury PT, and Sulzer D. Impaired degradation of mutant alpha-synuclein by chaperone-mediated autophagy. *Science* 305: 1292–1295, 2004.
11. Deng H, Jankovic J, Guo Y, Xie W, and Le W. Small interfering RNA targeting the PINK1 induces apoptosis in dopaminergic cells SH-SY5Y. *Biochem Biophys Res Commun* 337: 1133–1138, 2005.
12. Fernagut PO and Chesselet MF. Alpha-synuclein and transgenic mouse models. *Neurobiol Dis* 17: 123–130, 2004.
13. Friedlander R, Jarosch E, Urban J, Volkwein C, and Sommer T. A regulatory link between ER-associated protein degradation and the unfolded-protein response. *Nat Cell Biol* 2: 379–384, 2000.
14. Gee P and Davison AJ. Intermediates in the aerobic autoxidation of 6-hydroxydopamine: relative importance under different reaction conditions. *Free Radic Biol Med* 6: 271–284, 1989.
15. Ghee M, Fournier A, and Mallet J. Rat alpha-synuclein interacts with Tat binding protein 1, a component of the 26S proteasomal complex. *J Neurochem* 75: 2221–2224, 2000.
16. Holtz WA and O'Malley KL. Parkinsonian mimetics induce aspects of unfolded protein response in death of dopaminergic neurons. *J Biol Chem* 278: 19367–19377, 2003.
17. Imai Y, Soda M, Hatakeyama S, Akagi T, Hashikawa T, Nakayama KI, and Takahashi R. CHIP is associated with Parkin, a gene responsible for familial Parkinson's disease, and enhances its ubiquitin ligase activity. *Mol Cell* 10: 55–67, 2002.
18. Imai Y, Soda M, Inoue H, Hattori N, Mizuno Y, and Takahashi R. An unfolded putative transmembrane polypeptide, which can lead to endoplasmic reticulum stress, is a substrate of Parkin. *Cell* 105: 891–902, 2001.
19. Imai Y, Soda M, and Takahashi R. Parkin suppresses unfolded protein stress-induced cell death through its E3 ubiquitin–protein ligase activity. *J Biol Chem* 275: 35661–35664, 2000.
20. Kitada T, Asakawa S, Hattori N, Matsumine H, Yamamura Y, Minoshima S, Yokochi M, Mizuno Y, and Shimizu N. Mutations in the parkin gene cause autosomal recessive juvenile parkinsonism. *Nature* 392: 605–608, 1998.
21. Kitao Y, Imai Y, Ozawa K, Kataoka A, Ikeda T, Soda M, Namekawa K, Kiyama H, Stern DM, Hori O, Wakamatsu K, Ito S, Itohara S, Takahashi R, and Ogawa S. Pael receptor induces death of dopaminergic neurons in the substantia nigra via endoplasmic reticulum stress and dopamine toxicity, which is enhanced under condition of parkin inactivation. *Hum Mol Genet* 16: 50–60, 2007.
22. Kondo S, Murakami T, Tatsumi K, Ogata M, Kanemoto S, Otori K, Iseki K, Wanaka A, and Imaizumi K. OASIS, a CREB/ATF-family member, modulates UPR signalling in astrocytes. *Nat Cell Biol* 7: 186–194, 2005.
23. Kruger R, Kuhn W, Muller T, Woitalla D, Graeber M, Kosel S, Przuntek H, Epplen JT, Schols L, and Riess O. Ala30Pro mutation in the gene encoding alpha-synuclein in Parkinson's disease. *Nat Genet* 18: 106–108, 1998.
24. LaVoie MJ, Ostaszewski BL, Weihofen A, Schlossmacher MG, and Selkoe DJ. Dopamine covalently modifies and functionally inactivates parkin. *Nat Med* 11: 1214–1221, 2005.
25. Ledesma MD, Galvan C, Hellias B, Dotti C, and Jensen PH. Astrocytic but not neuronal increased expression and redistribution of parkin during unfolded protein stress. *J Neurochem* 83: 1431–1440, 2002.
26. Lindholm D, Wootz H, and Korhonen L. ER stress and neurodegenerative diseases. *Cell Death Differ* 13: 385–392, 2006.
27. Lo Bianco C, Schneider BL, Bauer M, Sajadi A, Brice A, Iwatsubo T, and Aebischer P. Lentiviral vector delivery of parkin prevents dopaminergic degeneration in an alpha-synuclein rat model of Parkinson's disease. *Proc Natl Acad Sci USA* 101: 17510–17515, 2004.
28. Marciniak SJ, Yun CY, Oyadomari S, Novoa I, Zhang Y, Jungreis R, Nagata K, Harding HP, and Ron D. CHOP induces death by promoting protein synthesis and oxidation in the stressed endoplasmic reticulum. *Genes Dev* 18: 3066–3077, 2004.
29. Mori K. Tripartite management of unfolded proteins in the endoplasmic reticulum. *Cell* 101: 451–454, 2000.
30. Mouradian MM. Recent advances in the genetics and pathogenesis of Parkinson disease. *Neurology* 58: 179–185, 2002.
31. Murata S, Minami Y, Minami M, Chiba T, and Tanaka K. CHIP is a chaperone-dependent E3 ligase that ubiquitylates unfolded protein. *EMBO Rep* 2: 1133–1138, 2001.
32. Nagamori I, Yabuta N, Fujii T, Tanaka H, Yomogida K, Nishimune Y, and Nojima H. Tisp40, a spermatid specific bZip transcription factor, functions by binding to the unfolded protein response element via the Rip pathway. *Genes Cells* 10: 575–594, 2005.
33. Nishitoh H, Matsuzawa A, Tobiume K, Saegusa K, Takeda K, Inoue K, Hori S, Kakizuka A, and Ichijo H. ASK1 is essential for endoplasmic reticulum stress-induced neuronal cell death triggered by expanded polyglutamine repeats. *Genes Dev* 16: 1345–1355, 2002.
34. Oyadomari S, Yun C, Fisher EA, Kreglinger N, Kreibich G, Oyadomari M, Harding HP, Goodman AG, Harant H, Garrison JL, Taunton J, Katze MG, and Ron D. Cotranslocational degradation protects the stressed endoplasmic reticulum from protein overload. *Cell* 126: 727–739, 2006.
35. Paisan-Ruiz C, Jain S, Evans EW, Gilks WP, Simon J, van der Brug M, Lopez de Munain A, Aparicio S, Gil AM, Khan N, Johnson J, Martinez JR, Nicholl D, Carrera IM, Pena AS, de Silva R, Lees A, Marti-Masso JF, Perez-Tur J, Wood NW, and Singleton AB. Cloning of the gene containing mutations that cause PARK8-linked Parkinson's disease. *Neuron* 44: 595–600, 2004.
36. Plemper RK, Deak PM, Otto RT, and Wolf DH. Re-entering the translocon from the lumenal side of the endoplasmic reticulum. Studies on mutated carboxypeptidase yscY species. *FEBS Lett* 443: 241–245, 1999.
37. Plemper RK and Wolf DH. Endoplasmic reticulum degradation. Reverse protein transport and its end in the proteasome. *Mol Biol Rep* 26: 125–130, 1999.
38. Plemper RK and Wolf DH. Retrograde protein translocation: ERADication of secretory proteins in health and disease. *Trends Biochem Sci* 24: 266–270, 1999.
39. Polymeropoulos MH, Lavedan C, Leroy E, Ide SE, Dehejia A, Dutra A, Pike B, Root H, Rubenstein J, Boyer R, Stenroos ES, Chandrasekharappa S, Athanassiadou A, Papapetropoulos T, Johnson WG, Lazzarini AM, Duvoisin RC, Di Iorio G, Golbe LI, and Nussbaum RL. Mutation in the alpha-synuclein gene identified in families with Parkinson's disease. *Science* 276: 2045–2047, 1997.
40. Rao RV and Bredesen DE. Misfolded proteins, endoplasmic reticulum stress and neurodegeneration. *Curr Opin Cell Biol* 16: 653–662, 2004.
41. Reinheckel T, Ullrich O, Sitte N, and Grune T. Differential impairment of 20S and 26S proteasome activities in human hematopoietic K562 cells during oxidative stress. *Arch Biochem Biophys* 377: 65–68, 2000.
42. Ryu EJ, Harding HP, Angelastro JM, Vitolo OV, Ron D, and Greene LA. Endoplasmic reticulum stress and the unfolded protein response in cellular models of Parkinson's disease. *J Neurosci* 22: 10690–10698, 2002.
43. Schroder M and Kaufman RJ. ER stress and the unfolded protein response. *Mutat Res* 569: 29–63, 2005.
44. Schroder M and Kaufman RJ. The mammalian unfolded protein response. *Annu Rev Biochem* 74: 739–789, 2005.
45. Selkoe DJ. Folding proteins in fatal ways. *Nature* 426: 900–904, 2003.

46. Singleton AB, Farrer M, Johnson J, Singleton A, Hague S, Kachergus J, Hulihan M, Peuralinna T, Dutra A, Nussbaum R, Lincoln S, Crawley A, Hanson M, Maraganore D, Adler C, Cookson MR, Muenter M, Baptista M, Miller D, Blancato J, Hardy J, and Gwinn–Hardy K. alpha-Synuclein locus triplication causes Parkinson's disease. *Science* 302: 841, 2003.
47. Smith WW, Jiang H, Pei Z, Tanaka Y, Morita H, Sawa A, Dawson VL, Dawson TM, and Ross CA. Endoplasmic reticulum stress and mitochondrial cell death pathways mediate A53T mutant alpha-synuclein-induced toxicity. *Hum Mol Genet* 14: 3801–3811, 2005.
48. Spillantini MG, Schmidt ML, Lee VM, Trojanowski JQ, Jakes R, and Goedert M. Alpha-synuclein in Lewy bodies. *Nature* 388: 839–840, 1997.
49. Springer W and Kahle PJ. Mechanisms and models of alpha-synuclein-related neurodegeneration. *Curr Neurol Neurosci Rep* 6: 432–436, 2006.
50. Stefanis L, Larsen KE, Rideout HJ, Sulzer D, and Greene LA. Expression of A53T mutant but not wild-type alpha-synuclein in PC12 cells induces alterations of the ubiquitin-dependent degradation system, loss of dopamine release, and autophagic cell death. *J Neurosci* 21: 9549–9560, 2001.
51. Tanaka Y, Engelender S, Igarashi S, Rao RK, Wanner T, Tanzi RE, Sawa A, V LD, Dawson TM, and Ross CA. Inducible expression of mutant alpha-synuclein decreases proteasome activity and increases sensitivity to mitochondria-dependent apoptosis. *Hum Mol Genet* 10: 919–926, 2001.
52. Valente EM, Abou–Sleiman PM, Caputo V, Muqit MM, Harvey K, Gispert S, Ali Z, Del Turco D, Bentivoglio AR, Healy DG, Albanese A, Nussbaum R, Gonzalez–Maldonado R, Deller T, Salvi S, Cortelli P, Gilks WP, Latchman DS, Harvey RJ, Dallapiccola B, Auburger G, and Wood NW. Hereditary early-onset Parkinson's disease caused by mutations in PINK1. *Science* 304: 1158–1160, 2004.
53. Webb JL, Ravikumar B, Atkins J, Skepper JN, and Rubinsztein DC. Alpha-Synuclein is degraded by both autophagy and the proteasome. *J Biol Chem* 278: 25009–25013, 2003.
54. Yamamuro A, Yoshioka Y, Ogita K, and Maeda S. Involvement of endoplasmic reticulum stress on the cell death induced by 6-hydroxydopamine in human neuroblastoma SH-SY5Y cells. *Neurochem Res* 31: 657–664, 2006.
55. Yang Y, Nishimura I, Imai Y, Takahashi R, and Lu B. Parkin suppresses dopaminergic neuron-selective neurotoxicity induced by Pael-R in Drosophila. *Neuron* 37: 911–924, 2003.
56. Yao D, Gu Z, Nakamura T, Shi ZQ, Ma Y, Gaston B, Palmer LA, Rockenstein EM, Zhang Z, Masliah E, Uehara T, and Lipton SA. Nitrosative stress linked to sporadic Parkinson's disease: *S*-nitrosylation of parkin regulates its E3 ubiquitin ligase activity. *Proc Natl Acad Sci USA* 101: 10810–10814, 2004.
57. Zhang K, Shen X, Wu J, Sakaki K, Saunders T, Rutkowski DT, Back SH, and Kaufman RJ. Endoplasmic reticulum stress activates cleavage of CREBH to induce a systemic inflammatory response. *Cell* 124: 587–599, 2006.
58. Zhao L and Ackerman SL. Endoplasmic reticulum stress in health and disease. *Curr Opin Cell Biol* 18: 444–452, 2006.
59. Zimprich A, Biskup S, Leitner P, Lichtner P, Farrer M, Lincoln S, Kachergus J, Hulihan M, Uitti RJ, Calne DB, Stoessl AJ, Pfeiffer RF, Patenge N, Carbajal IC, Vieregge P, Asmus F, Muller–Myhsok B, Dickson DW, Meitinger T, Strom TM, Wszolek ZK, and Gasser T. Mutations in LRRK2 cause autosomal-dominant parkinsonism with pleomorphic pathology. *Neuron* 44: 601–607, 2004.

Address reprint requests to:
Ryosuke Takahashi, M.D.
Department of Neurology
Kyoto University Graduate School of Medicine
54 Kawahara-cho, Shogoin, Sakyo-ku,
Kyoto 606-8507, Japan

E-mail: ryosuket@kuhp.kyoto-u.ac.jp

Date of first admission to ARS Central, December 1, 2006; date of acceptance, December 5, 2006.

Available online at www.sciencedirect.com
ScienceDirect
Neuroscience Letters 417 (2007) 128–131
Neuroscience Letters
www.elsevier.com/locate/neulet

Capillary beds are decreased in Alzheimer's disease, but not in Binswanger's disease

Hiroshi Kitaguchi[a], Masafumi Ihara[a], Hidemoto Saiki[b], Ryosuke Takahashi[a], Hidekazu Tomimoto[a,*]

[a] *Department of Neurology, Graduate School of Medicine, Kyoto University, Sakyo-ku, Kyoto 606-8507, Japan*
[b] *Department of Neurology, Kitano Hospital, Tazuke Kofukai Medical Research Institute, Osaka 530-8480, Japan*

Received 1 December 2006; received in revised form 23 January 2007; accepted 6 February 2007

Abstract

Morphological abnormalities of the cortical microvessels have been reported in Alzheimer's disease (AD), but not in Binswanger's disease (BD), a form of vascular dementia. Therefore, we compared the capillary beds in AD and BD brains, using a modified Gallyas silver impregnation method and immunohistochemistry for β amyloid. Eight autopsied brains with AD and seven with BD were compared with six control brains. The cortical microvessels in AD were frequently narrowed, and torn off, especially in close proximity to the senile plaques. The capillary densities in AD were significantly decreased as compared with the control brains. In contrast, there were no significant changes in the capillary densities and their morphologies in BD brains. Immunohistochemistry for β amyloid revealed numerous deposits in the vascular wall and perivascular neuropil exclusively in AD brains. Cortical microvascular changes in AD and their absence in BD may indicate a role of β amyloid for the microvessel pathology in AD.

Keywords: Microvessel; Alzheimer's disease; Vascular dementia; Binswanger's disease; Silver impregnation; Amyloid protein

Alzheimer's disease (AD) and vascular dementia are major causes of dementia and disabilities in the elderly. These two conditions have been believed to have an independent pathoetiology. However, in recent studies, co-morbid factors have been revealed in AD and vascular dementia [10,12]. These factors include hypertension, diabetes mellitus, hyperlipidemia, apo E4 ε genotype, cholinergic deficits, and white matter lesions. In addition, patients with vascular lesions reportedly develop dementia more frequently than those without vascular lesions among those subjects with senile changes [18]. Taken together, this evidence has shed light on the interrelationship between AD and vascular dementia, and raised the hypothesis that vascular factors may have a role in the pathogenesis of AD. In concordance with this hypothesis, previous electron microscopic studies have reported thickening of the basement membrane, denervation of the perivascular nerves, and bulging or narrowing of the cortical microvessels in AD brains [14,17].

Binswanger's disease (BD) is a form of vascular dementia, featured by diffuse white matter lesions, lacunar infarcts and fibrohyaline thickening of the microvessel [13]. Fibrohyaline thickening of the microvessels is marked in BD, and significant but less severe in AD in the cerebral white matter [19]. However, with respect to the cortical microvessels, there are no studies in BD. Therefore, we aimed to compare the alterations of the cortical microvessels in AD and BD using a modified Gallyas silver impregnation method and immunohistochemistry for β amyloid, which enable us to examine the network of the brain capillaries, and senile plaques.

We examined 21 brains, including 8 from patients with AD (3 males), 7 from patients with BD (4 males), and 6 from patients who did not have any neuropsychiatric symptoms or brain lesions (3 males). The age was 79 ± 12 years (mean ± S.D.) in the AD, 74 ± 13 years in the BD and 73 ± 4 in the control groups, respectively, among which no significant differences were observed ($p < 0.05$). The brain weight was 1020 ± 111 g in the AD, 1093 ± 112 g in the BD, and 1244 ± 57 g in the control groups, respectively. The brain weight in the AD group was significantly lower than in the control and BD groups ($p < 0.05$). The patients with AD and BD, but not the control patients, met

* Corresponding author. Tel.: +81 75 751 3766; fax: +81 75 751 3766.
E-mail address: tomimoto@kuhp.kyoto-u.ac.jp (H. Tomimoto).

0304-3940/$ – see front matter © 2007 Elsevier Ireland Ltd. All rights reserved.
doi:10.1016/j.neulet.2007.02.021

the diagnostic criteria for dementia (diagnostic and statistical manual of mental disorders; DSM-IV) [1] in the occasion of diagnosis and, most of these patients suffered in a bed-ridden condition in their terminal stages.

The diagnosis of AD was made based on the Consortium to Establish a Registry for Alzheimer's Disease (CERAD) diagnostic neuropathologic criteria [15] and excluded the brains with large cerebral infarctions. The diagnosis of BD was made clinico-pathologically, and retrospectively met the pathological inclusion criteria including (1) presence of diffuse white matter lesions, (2) lacunar infarctions in the perforator territory, (3) arteriolosclerosis such as fibrohyalinosis and fibrinoid necrosis and (4) absence of cortical infarctions, as well as the clinical criteria by Bennett et al. [3], and excluded the brains with significant pathologic hallmarks of AD. The control group included two patients with pneumonia, one patient each with renal cancer, lung cancer, chronic renal failure and pulmonary emphysema.

The tissue blocks were sectioned in a cryostat (30 or 100 μm-thick) and kept in 0.1 M phosphate buffer (pH 7.4). The tissue sections were processed according to the silver impregnation method described by Gallyas [8]. Briefly, the sections were incubated for 30 min in 5% periodic acid (HIO4) solution. The sections were then immersed in 4% sodium hydroxide solution for 30 min, and washed in 0.5% acetic acid solution in double-distilled water for 5 min. They were further incubated in a mixture (pH 13.0) of 90 ml of an ammoniated silver nitrate solution (AgNO3, 0.5 g and ammonium nitrate, 2.5 g in 900 ml double-distilled water), and 10 ml of 4% sodium dihydroxide in double-distilled water for 30 min at 20 °C. These sections were left in a physical developer solution, which was composed of a mixture of 10 ml of solution A, 5 ml of solution B and 5 ml of solution C at 25 °C. The composition of each solution was as follows; sodium carbonate, 50 g in 1000 ml of distilled water (solution A); ammonium nitrate 1.9 g, silver nitrate, 2.0 g; tungsto-silicic acid ($SiO_2 \cdot 2WO_3$), 10 g in 1000 ml of distilled water (solution B); and ammonium nitrate, 1.9 g; silver nitrate, 2.0 g; tungsto-silicic acid ($SiO_2 \cdot 2WO_3$), 10.0 g; and 6.1 ml of 40% formalin solution in 1000 ml of distilled water (solution C). The reaction was terminated in 0.5% acetic acid solution, and the extent of silver impregnation was monitored intermittently under light microscopy.

For immunohistochemistry, autoclaved paraffin sections were incubated with a mouse anti-amyloid β protein antibody (Dakopatts, diluted 1:200), biotinylated anti mouse IgG (Vector laboratories, diluted 1:200) and an avidin biotinylated peroxidase complex (Vector Laboratories, diluted 1:200). They were finally visualized with 0.01% diaminobenzidine tetrahydrochloride and 0.005% H_2O_2 in 0.05 M Tris–HCl (pH 7.6). To test for the specificity of the immunohistochemical reaction, control sections were incubated with normal mouse IgG instead of the primary antibody.

The density of the capillary beds was determined by the test grid method [7], in which the number of vascular intersections were counted against 6 × 6 square test grids each with a 50 μm width. The average counts from five representative fields in the layers II–IV of the frontal and parietal cortices, respectively, were used as the capillary densities in each patient. The data were expressed as means ± S.D. and the Mann–Whitney *U*-test was used to compare between the groups.

Using the modified Gallyas stains, the microvessels in the cerebral cortices appeared smooth and regular in diameter in the non-neurological control and BD brains (Fig. 1A and C, respectively). There were no senile plaques nor neurofibrillary tangles. In contrast, the brains with AD had numerous senile plaques and neurofibrillary tangles, which were intermingled by irregularly-shaped microvessels in both frontal and parietal cortices (Fig. 1B). The microvessels were frequently narrowed and irregular in diameter for a variable length of the vessel (Fig. 1D–F). These vessels often showed bulging of their walls. In close proximity to the senile plaques, the microvessels were blunted and torn off in the sections with a thickness of 100 μm (Fig. 1E). These microscopic changes were not observed in the non-neurological control and BD groups.

With immunohistochemistry, β amyloid-immunoreactivity was localized in senile plaques which accumulated numerously in the superficial layer, as well as perivascular deposits in the vascular wall itself and perivascular neuropil in the AD group (Fig. 1G–I). Beta amyloid-immunopositive fine texture fibrils were distributed in the neuropil with or without contact to the microvessels. In contrast, there was almost no deposit of β amyloid in the cerebral cortices of the non-neurological control and BD groups. In the semi-quantitative measures of the microvessels, the microvascular densities were significantly lower in the AD group as compared to the other two groups in both frontal and parietal cortices (Fig. 2).

The capillaries in AD have been shown to exhibit thickening of their basement membrane, atrophy, perivascular fibrosis and degeneration of the pericytes [5,6,16], which may correspond to the bulging of the microvessels observed here. In semi-quantitative measures, some authors have not observed any decrease in the capillary densities [2], while others showed a decrease in selected or non-selected regions of AD brains [4,7]. The present study underscored the morphological abnormalities of the capillaries, and further revealed their numerical decrease in AD and absence of capillary damages in BD. The actual reduction rate in the capillary density of AD brains may be more severe, because significant atrophy in this group should have ameliorated the reduction ratio. The fact that there were no β amyloid-deposits nor damages in the cortical microvessels in BD brains was not contradictory to the major site of the pathologic process, which involve subcortical white matter and perforator territory in BD. However, in previous studies, slight but significant neuronal dysfunction has been noted in the cerebral cortex, such as a decrease in the synaptic densities and neuronal viabilities [11,22].

The reduction in the vascular densities and the spatial proximity of β amyloid deposits to the microvascular changes may suggest some vascular toxicity due to β amyloid. Indeed, preamyloid deposits were found in the extracellular space and extended directly into the capillaries [16]. Vinters and Farag [20] raised a neurovascular hypothesis, in which β amyolid accumulates on the outer side of the basement membrane and

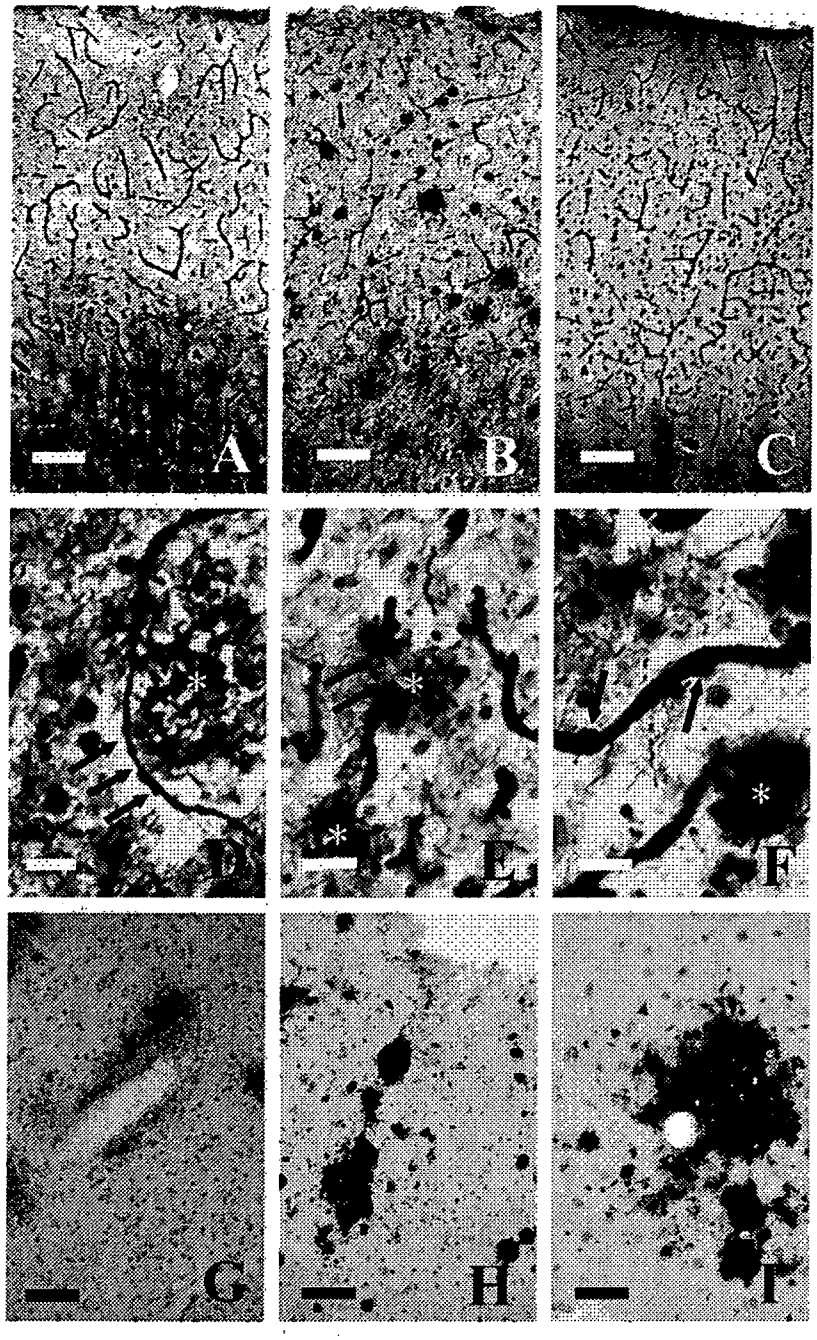

Fig. 1. Photomicrograph of Gallyas stains (A)–(F) and immunohistochemistry for β amyloid (G)–(I). The photographs were taken in the cerebral cortex of non-neurological (A); AD (B), (D)–(I); and BD patients (C). Numerous senile plaques (asterisks) were observed exclusively in AD brains. The capillary density appears less dense in AD as compared with the non-neurological and BD brains. The small vessels showed narrowing (arrows in D), tearing off (arrows in E) and scattered bulging (arrows in F). There were perivascular deposit in the vascular wall which extended into the neuropil diffusely (G). A heavy accumulation of perivascular β amyloid was also seen in the tangential (H) and axial planes (I), in which the perivascular deposits continued into the neuroglial deposits. Bars indicate 100 μm for (A)–(C), (I), 30 μm for (D)–(F) and 200 μm in (G), (H).

may promote local neurovascular inflammation. In support for this hypothesis, GAX, a gene encoding a homeodomain-transcription factor box gene related to vascular differentiation [9], is downregulated in AD brains. The downregulation of GAX activates a proapoptotic pathway, and may result in a decrease in the number of cerebral microvessels and cerebral blood flow (CBF), by way of activating the forkhead transcription factor, AFX-1. This activation may also downregulate low density lipoprotein receptor-related prtoein-1 (LRP) which enhances efflux of β amyloid from the brain [21]. This impaired clearance of β amyloid may further increase soluble β amyloid and fibrillary β amyloid levels [23]. Finally, we hypothesized a vicious cycle in which β amyloid may cause microvascular regression, brain hypoperfusion and neurovascular inflammation, although this will be addressed in future studies.

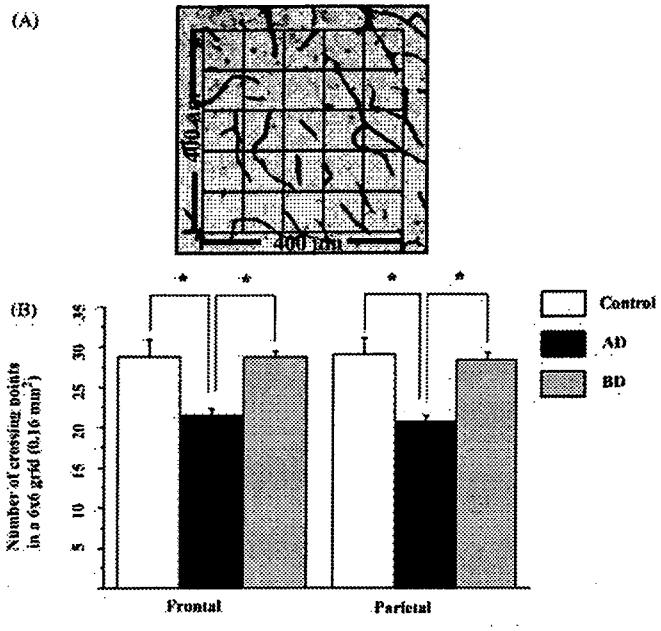

Fig. 2. Quantitative evaluation of capillary densities in the cerebral cortex. (A) indicates the grid applied for a non-neurological control brain; (B) indicates the capillary densities in the non-neurological, AD and BD brains. $*p < 0.05$ by Mann–Whitney U-test.

Acknowledgement

This study was supported in part by a grant-in-aid for scientific research (C) (18590936) from the Japanese Ministry of Education, Culture, Sports, Science and Technology to H. S. and H. T.

References

[1] American Psychiatric Association, Diagnostic and Statistical Manual of Mental Disorders, fourth ed., Washington, DC, American Psychiatric Association, 1994.
[2] M.A. Bell, M.J. Ball, Morphometric comparison of hippocampal microvasculature in ageing and demented people: diameters and densities, Acta Neuropathol. 53 (1981) 299–318.
[3] D.A. Bennett, R.S. Wilson, D.W. Gilley, J.H. Fox, Clinical diagnosis of Binswanger's disease, J. Neurol. Neurosurg. Psychiatry 53 (1990) 961–965.
[4] L. Buee, P.R. Hof, C. Bouras, A. Delacourte, D.P. Perl, J.H. Morrison, H.M. Fillit, Pathological alterations of the cerebral microvasculature in Alzheimer's disease and related dementing disorders, Acta Neuropathol. 87 (1994) 469–480.
[5] J.C. de la Torre, Hemodynamic consequences of deformed microvessels in the brain in Alzheimer's disease, Ann. N Y Acad. Sci. 826 (1997) 75–91.
[6] E. Farkas, P.G. Luiten, Cerebral microvascular pathology in aging and Alzheimer's disease, Prog. Neurobiol. 64 (2001) 575–611.
[7] V.W. Fischer, A. Siddiqi, Y. Yusufaly, Altered angioarchitecture in selected areas of brains with Alzheimer's disease, Acta Neuropathol. 79 (1990) 672–679.
[8] F. Gallyas, Silver staining of collagen and reticulin fibers and cerebral capillaries by mean of physical development, J. Microscopy 91 (1970) 119–124.
[9] D.H. Gorski, K. Walsh, Control of vascular cell differentiation by homeobox transcription factors, Trends Cardiovasc. Med. 13 (2003) 213–220.
[10] V. Hachinski, D.G. Munoz, Cerebrovascular pathology in Alzheimer's disease: cause, effect or epiphenomenon? Ann. N Y Acad. Sci. 826 (1997) 1–6.
[11] M. Ihara, H. Tomimoto, K. Ishizu, T. Mukai, H. Yoshida, N. Sawamoto, M. Inoue, T. Doi, K. Hashikawa, J. Konishi, H. Shibasaki, H. Fukuyama, Decrease in cortical benzodiazepine receptors in symptomatic patients with leukoaraiosis: a positron emission tomography study, Stroke 35 (2004) 942–947.
[12] R.N. Kalaria, Similarities between Alzheimer's disease and vascular dementia, J. Neurol. Sci. 203–204 (2002) 29–34.
[13] J.-Xi. Lin, H. Tomimoto, I. Akiguchi, M. Matsuo, H. Wakita, H. Shibasaki, H. Budka, Vascular cell components of the medullary arteries in Binswanger's disease brains; a morphometric and immunoelectron microscopic study, Stroke 31 (2000) 1838–1842.
[14] G.L. Mancardi, F. Perdelli, C. Rivano, A. Leonardi, O. Bugiani, Thickening of the basement membrane of cortical capillaries in Alzheimer's disease, Acta Neuropathol. 49 (1980) 79–83.
[15] S.S. Mirra, A. Heyman, D. McKeel, S.M. Sumi, B.J. Crain, L.M. Brownlee, F.S. Vogel, J.P. Hughes, G. van Belle, L. Berg, The Consortium to Establish a Registry for Alzheimer's Disease (CERAD). Part II. Standardization of the neuropathologic assessment of Alzheimer's disease, Neurology 41 (1991) 479–486.
[16] T. Miyakawa, S. Katsuragi, K. Yamashita, K. Ohuchi, Morphological study of amyloid fibrils and preamyloid deposits in the brain with Alzheimer's disease, Acta Neuropathol. 83 (1992) 340–346.
[17] A.B. Scheibel, Alterations of the cerebral capillary bed in the senile dementia of Alzheimer, Ital. J. Neurol. Sci. 8 (1987) 457–463.
[18] D.A. Snowdon, L.H. Greiner, J.A. Mortimer, K.P. Riley, P.A. Greiner, W.R. Markesbery, Brain infarction and the clinical expression of Alzheimer disease, JAMA 277 (1997) 813–817.
[19] H. Tomimoto, I. Akiguchi, H. Akiyama, K. Ikeda, H. Wakita, J.-Xi. Lin, I. Akiguchi, M. Kinoshita, H. Shibasaki, Vascular changes in white matter lesions of Alzheimer's disease, Acta Neuropathol. 97 (1999) 629–634.
[20] H.V. Vinters, E.S. Farag, Amyloidosis of cerebral arteries, Adv. Neurol. 92 (2003) 105–112.
[21] Z. Wu, H. Guo, N. Chow, J. Sallstrom, R.D. Bell, R. Deane, A.I. Brooks, S. Kanagala, A. Rubio, A. Sagare, D. Liu, F. Li, D. Armstrong, T. Gasiewicz, R. Zidovetzki, X. Song, F. Hofman, B.V. Zlokovic, Role of the MEOX2 homeobox gene in neurovascular dysfunction in Alzheimer disease, Nat. Med. 11 (2005) 959–965.
[22] S.S. Zhan, K. Beyreuther, H.P. Schmitt, Synaptophysin immunoreactivity of the cortical neuropil in vascular dementia of Binswanger type compared with the dementia of Alzheimer type and nondemented controls, Dementia 5 (1994) 79–87.
[23] B.V. Zlokovic, Neurovascular mechanisms of Alzheimer's neurodegeneration, Trends Neurosci. 28 (2005) 202–208.

Available online at www.sciencedirect.com
ScienceDirect
Biochemical and Biophysical Research Communications 356 (2007) 993–997
BBRC
www.elsevier.com/locate/ybbrc

Evolution of mitochondrial cell death pathway: Proapoptotic role of HtrA2/Omi in *Drosophila*

Tatsushi Igaki [a,1], Yasuyuki Suzuki [b,1], Naoko Tokushige [c], Hiroka Aonuma [d,f], Ryosuke Takahashi [e,*], Masayuki Miura [f,*]

[a] *Department of Genetics, Yale University School of Medicine, Boyer Center for Molecular Medicine, 295 Congress Avenue, New Haven, CT 06536, USA*
[b] *Department of Degenerative Neurological Diseases, National Institute of Neuroscience, National Center of Neurology and Psychiatry, Kodaira, Tokyo 187-8502, Japan*
[c] *Laboratory for Developmental Neurobiology, Brain Science Institute, RIKEN, 2-1 Hirosawa, Wako, Saitama 351-0198, Japan*
[d] *Laboratories for Integrated Biology, Graduate School of Frontier Biosciences, Osaka University, 1-3 Yamadaoka, Suita, Osaka 565-0871, Japan*
[e] *Department of Neurology, Kyoto University Graduate School of Medicine, 54 Shogoin-Kawaharacho, Sakyoku, Kyoto 606-8507, Japan*
[f] *Department of Genetics, Graduate School of Pharmaceutical Sciences, University of Tokyo, 7-3-1 Hongo, Bunkyo-ku, Tokyo 113-0033, Japan*

Received 14 March 2007
Available online 26 March 2007

Abstract

Despite the essential role of mitochondria in a variety of mammalian cell death processes, the involvement of mitochondrial pathway in *Drosophila* cell death has remained unclear. To address this, we cloned and characterized DmHtrA2, a *Drosophila* homolog of a mitochondrial serine protease HtrA2/Omi. We show that DmHtrA2 normally resides in mitochondria and is up-regulated by UV-irradiation. Upon receipt of apoptotic stimuli, DmHtrA2 is translocated to extramitochondrial compartment; however, unlike its mammalian counterpart, the extramitochondrial DmHtrA2 does not diffuse throughout the cytosol but stays near the mitochondria. RNAi-mediated knock-down of DmHtrA2 in larvae or adult flies results in a resistance to stress stimuli. DmHtrA2 specifically cleaves *Drosophila* inhibitor-of-apoptosis protein 1 (DIAP1), a cellular caspase inhibitor, and induces cell death both *in vitro* and *in vivo* as potent as other fly cell death proteins. Our observations suggest that DmHtrA2 promotes cell death through a cleavage of DIAP1 in the vicinity of mitochondria, which may represent a prototype of mitochondrial cell death pathway in evolution.

Keywords: Apoptosis; Cell death; *Drosophila*; HtrA2/Omi; Mitochondria

Mitochondria play crucial roles in regulating cell death in mammals [1,2]. Upon receipt of apoptotic stimuli, the cell activates caspase protease cascade to execute cell death. The activation of caspases is largely regulated by mitochondrial proteins such as cytochrome *c* (cyt *c*), Smac/DIABLO, and HtrA2/Omi, which are released to cytosol following cell death stimuli [1,2]. cyt *c* directly activates the cytosolic caspase-activating protein Apaf-1, thereby triggering a cascade of caspase activations [1,3]. On the other hand, Smac/DIABLO and HtrA2/Omi indirectly activate caspases by antagonizing inhibitor-of-apoptosis proteins (IAPs), a family of cellular caspase inhibitors [4–7]. HtrA2/Omi, as well as cyt *c*, has also been shown to be important for cell survival, as loss of HtrA2/Omi gene results in a neurodegeneration in mice [8,9].

Despite abundant similarities in cell death mechanisms between vertebrates and flies, the involvement of mitochondria in *Drosophila* cell death machinery has remained unclear. *Drosophila* cell death is largely regulated by three killer proteins Reaper, Hid, and Grim. These proteins are thought to be functional counterparts of mammalian mitochondrial killer proteins Smac/DIABLO and HtrA2/Omi, as they bind to and antagonize IAPs through their

* Corresponding authors.
E-mail addresses: ryosuket@kuhp.kyoto-u.ac.jp (R. Takahashi), miura@mol.f.u-tokyo.ac.jp (M. Miura).
[1] These authors contributed equally to this work.

0006-291X/$ - see front matter © 2007 Elsevier Inc. All rights reserved.
doi:10.1016/j.bbrc.2007.03.079

conserved four-amino-acid sequences called RHG (Reaper, Hid, and Grim) motif or IBM (IAP-Binding Motif) [3,10]. Unlike mammalian counterparts, however, RHG normally reside in the cytoplasm and their activities are regulated either at transcriptional levels or by phosphorylation [11]. The presence of two *Drosophila* Bcl-2 family proteins that localize to mitochondria [12,13] indicates that mitochondrial cell death pathway may also exist in flies [14]. Here, in order to investigate the role of mitochondria in *Drosophila* cell death pathway, we cloned and characterized DmHtrA2, a *Drosophila* homolog of HtrA2/Omi. Our data suggest that DmHtrA2 promotes cell death through a cleavage of *Drosophila* IAP1 (DIAP1) in the vicinity of mitochondria, which may represent a prototype of mitochondrial cell death pathway in evolution.

Materials and methods

Stress resistance. For UV-resistance, third-instar larvae were irradiated with 5 mJ/cm^2 UV and allowed to develop at 25 °C. Paraquat resistance was tested essentially as described [15]. Adult flies (age 10–20 days) were starved for 6 h and transferred to vials containing two 2 cm × 2 cm filter squares wetted with 20 mM paraquat (Sigma) in 5% sucrose solution. Survival was scored at 18 or 24 h after the transfer. The ingestion rate was determined by dye intake by adding 10 mg/ml bromophenol blue instead of paraquat. Fly lysate was analyzed by monitoring the absorbance at 595 nm at 18 h.

Recombinant proteins and cleavage assay. The C-terminally His_6-tagged recombinant human HtrA2 protein (HsHtrA2ΔN133-His_6) was described previously [6]. The N-terminally GST-tagged recombinant DmHtrA2 protein (GST-DmHtrA2ΔN92) was produced in the *Escherichia coli*. The protein was purified by affinity chromatography using Glutathione Sepharose™ 4B (Amersham Bioscience). N-terminally FLAG-tagged DIAP1 or Hop was translated *in vitro* in the presence of [^{35}S]-methionine using a TNT T7 Quick Coupled Transcription/Translation System (Promega). [^{35}S]-labeled proteins were incubated with recombinant HtrA2 proteins (100 nM) in Tris buffer containing 50 mM Tris–HCl (pH 7.5), 150 mM NaCl, and 1 mM DTT for 1 h at 37 °C. The reaction mixtures were subjected to SDS–PAGE and visualized by autoradiography.

Cell death assay. Cell death assay was performed as described previously [12]. In brief, S2 cells were transfected with pUAST-derived expression constructs with a driver plasmid pWAGAL4 (actin promoter-GAL4), together with a reporter plasmid pCaspeR-hs-lacZ that encodes β-galactosidase under the control of the *hsp70* promoter. Twenty-four hours after transfection, the cells were heat-shocked at 37 °C and cultured for another 24 h. The cells were lysed at 48 h and assayed for β-galactosidase activity in a reaction mixture containing *o*-nitrophenyl-β-D-galactopyranoside.

For information regarding cloning, expression constructs, antibodies, cell culture, subcellular fractionation, Western blotting, and fly stocks, see Supplementary information.

Results and discussion

We cloned the DmHtrA2 cDNA (DDBJ/EMBL/GenBank, Accession No. AB112473) from the total RNA of wild-type fly embryo. DmHtrA2 encoded a protein of 422 amino acids with an N-terminal transmembrane (TM) domain, a central trypsin-like serine protease domain, and a C-terminal PDZ domain, as well as an IBM-like (ASKM) sequence that locates adjacent to the TM (Supplemental Fig. 1). RT-PCR analysis revealed that DmHtrA2 mRNA was expressed at all stages of *Drosophila* development (Supplemental Fig. 1).

To investigate the role of DmHtrA2 in cell death, we induced cell death in *Drosophila* S2 cells by UV-irradiation. Four hours after irradiation, the cells began to exhibit apoptotic morphological changes (Fig. 1A and B). We found that the protein level of DmHtrA2 was significantly up-regulated in the irradiated cells in a time-dependent

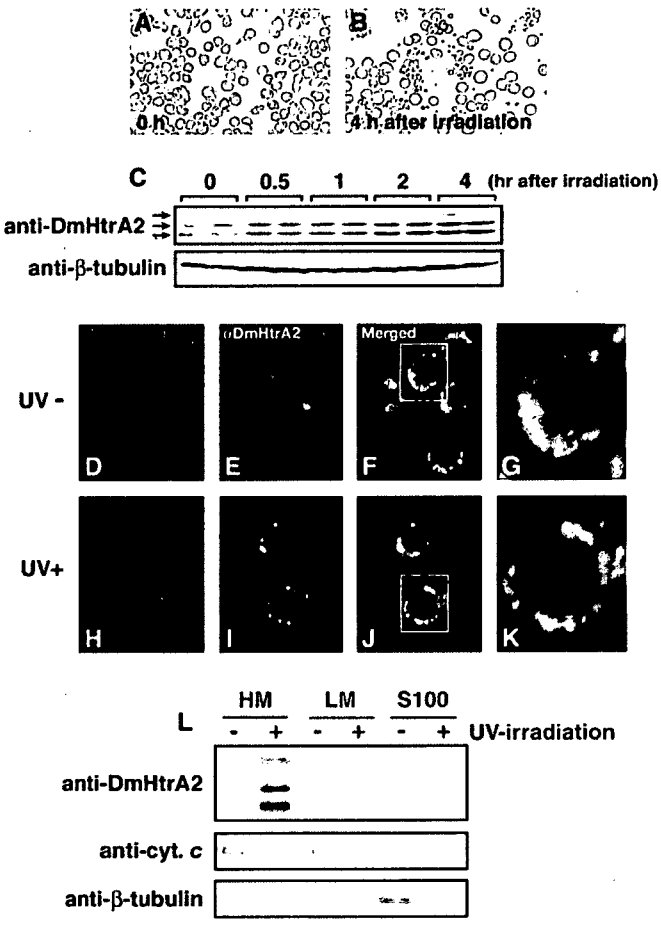

Fig. 1. Apoptotic stimulus up-regulates DmHtrA2 and induces its translocation from mitochondria to extramitochondrial compartment. (A,B) S2 cells were irradiated with UV (200 mJ/cm^2) and cultured for another 4 h. (C) Endogenous DmHtrA2 levels were assessed by Western blotting using an anti-DmHtrA2 antibody before and after UV-irradiation. An anti-β-tubulin antibody was used for a loading control. The anti-DmHtrA2 antibody recognized three bands; the highest band corresponded to the size of full-length form, and the lowest band corresponded to the size of putative mitochondrial mature (ΔN) form (C, upper panel). The experiments were performed using duplicate dishes and were repeated three times. (D–K) Confocal images of S2 cells co-stained with Mitotracker (magenta) and an anti-DmHtrA2 antibody (green). Mitochondria and the endogenous DmHtrA2 protein were visualized before (D–G) or 4 h after (H–K) UV-irradiation (200 mJ/cm^2). G and K show magnified images from F and J, respectively. (L) S2 cells were fractionated before (−) or 4 h after (+) UV-irradiation (200 mJ/cm^2), and the cell lysate was subjected to Western blot analysis using anti-DmHtrA2, anti-cytochrome *c*, and anti-β-tubulin antibodies. For DmHtrA2 protein, the total amount of protein from each fraction was adjusted to 2.5 μg. For cytochrome *c* and β-tubulin, the mitochondrial and cytosolic markers, respectively, an equal volume (10 μl) from each fraction was used for Western analysis.

manner (Fig. 1C). This up-regulation was observed even at 2 h after irradiation, preceding the morphological changes (Fig. 1C). Immunostaining of DmHtrA2 revealed that it exclusively localized to mitochondria under the normal condition (Fig. 1D–G). Four hours after UV-irradiation, the anti-DmHtrA2 staining still showed a punctate pattern with a higher signal intensity, but it no longer merged with the Mitotracker-labeled mitochondria (Fig. 1H–K). This suggests that DmHtrA2 is translocated to extramitochondrial conpartment in response to UV-irradiation. We further analyzed the subcellular localization of DmHtrA2 by fractionating S2 cell lysates before and after irradiation. DmHtrA2 protein was detected in the heavy membrane (HM) fraction, as was cyt *c*, but not in either the light membrane (LM) or cytosolic (S100) fraction (Fig. 1L). We found that UV-irradiation did not alter this distribution (Fig. 1L), suggesting that DmHtrA2 is released to the extramitochondrial compartment but stays in the vicinity of the mitochondria. Since no difference was observed in the mitochondrial membrane potential between control and UV-irradiated S2 cells (Fig. 1D and H; [16]), it is unlikely that the complementary staining of anti-DmHtrA2 and Mitotracker in irradiated cells was due to a loss of membrane potential in a subset of mitochondria.

To examine the physiological role of DmHtrA2, we generated DmHtrA2 knock-down flies using an RNAi construct of DmHtrA2 and a ubiquitous driver da-GAL4. In the knock-down larvae and adults, DmHtrA2 protein level was greatly reduced (Fig. 2A). The knock-down flies were viable and fertile with no detectable morphological abnormalities. We found that the DmHtrA2 knock-down larvae were more resistant to UV-induced lethality compared to control larvae (Fig. 2B). Furthermore, the DmHtrA2 knock-down adult flies were more resistant to dietary paraquat, a superoxide stress agent (Fig. 2C). The ingestion rate of the knock-down flies was not affected (data not shown). These observations suggest that DmHtrA2 is involved in stress-induced toxicity *in vivo*.

Mammalian HtrA2/Omi induces cell death by cleaving and thereby inactivating IAPs through its serine protease activity [4–7]. We therefore assumed that the stress-induced toxicity mediated by DmHtrA2 is through a cleavage of DIAP1. We performed an *in vitro* cleavage assay using recombinant DmHtrA2 and DIAP1 proteins, and found that both *Drosophila* and human HtrA2 proteins specifically cleaved DIAP1 (Fig. 3A). These HtrA2 proteins did not cleave a control protein FLAG-tagged Hop (Hsp70/Hsp90-organizing protein) (Fig. 3A). Thus, the specific serine protease activity of HtrA2/Omi is conserved in *Drosophila*.

Finally, we examined whether DmHtrA2 can kill the cell. Overexpression of DmHtrA2 in S2 cells significantly reduced their viability as potent as other *Drosophila* killer proteins such as Reaper (Fig. 3B and data not shown). This cell death could not be blocked by caspase inhibitors such as DIAP1, p35, or p49, similar to the one caused by human HtrA2/Omi [4,6]. We further examined the toxicity of DmHtrA2 *in vivo*. Overexpression of DmHtrA2 in developing *Drosophila* eye resulted in "no eye" phenotype (Fig. 3C), suggestive of an extensive cell death during development. This phenotype was also resistant to caspase inhibitors (Fig. 3C). Together, these data suggest that DmHtrA2 potently induces cell death through a cleavage of DIAP1.

Our observations suggest that stress stimuli such as UV-irradiation cause translocation of DmHtrA2 from mito-

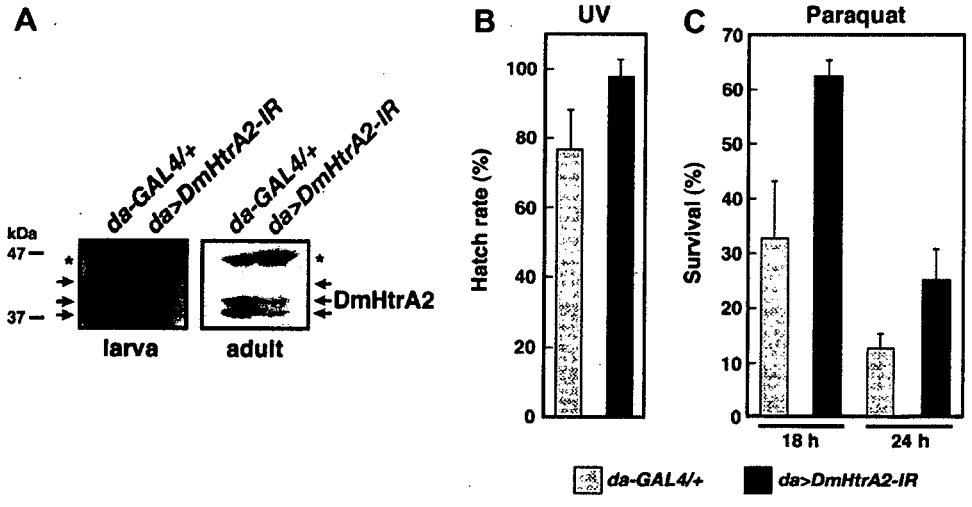

Fig. 2. DmHtrA2 mediates stress stimuli *in vivo*. (A) An RNAi construct (inverted-repeat; IR) for DmHtrA2 (UAS-DmHtrA2-IR) was driven by ubiquitous expression driver da-GAL4 in third-instar larvae or adult flies. Eight animals were homogenized with 96 μl of conventional SDS loading buffer and subjected to SDS–PAGE (4 μl/lane) followed by an anti-DmHtrA2 blotting. The non-specific bands detected by the anti-DmHtrA2 antibody (asterisks) show equal loadings of the protein. (B) Control (da-GAL4) or knock-down (da-GAL4, UAS-DmHtrA2-IR) third-instar larvae were irradiated with UV (5 mJ/cm^2), and the resistance was assessed by the number of adult flies that hatched. (C) Control or knock-down adult flies were starved and subjected to dietary paraquat. Survival was scored at 18 or 24 h after the beginning of ingestion.

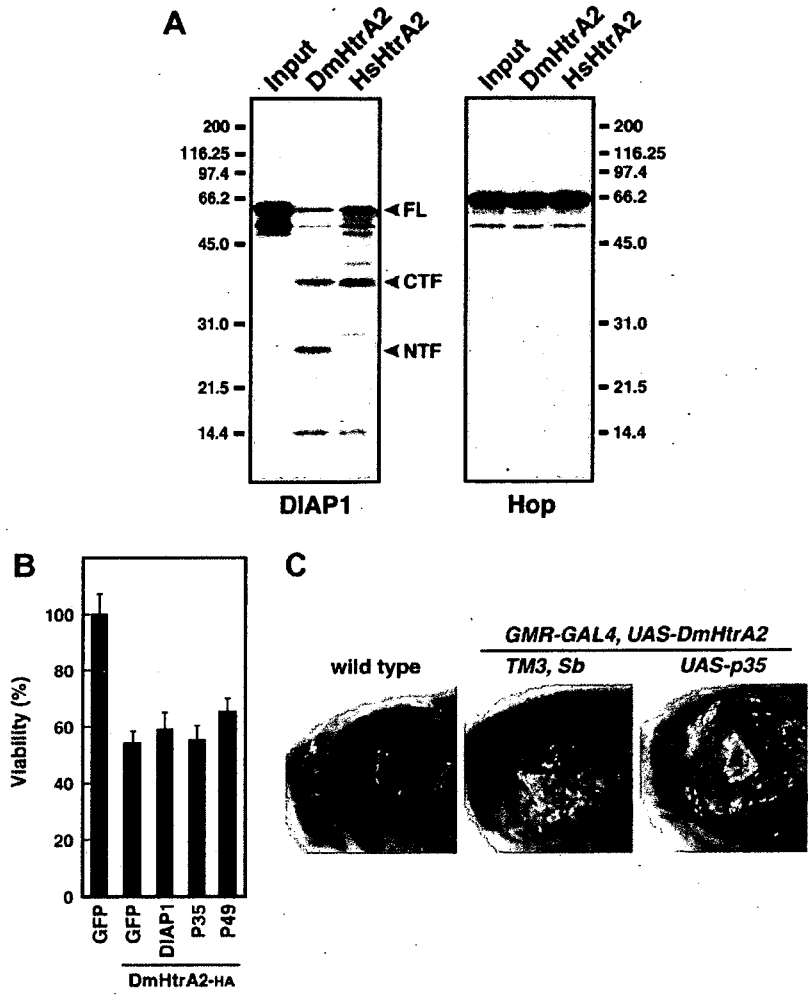

Fig. 3. DmHtrA2 is a potent cell death inducer that cleaves DIAP1. (A) [^{35}S]-labeled DIAP1 or Hop was incubated with *Drosophila* or human HtrA2 recombinant protein, subjected to SDS–PAGE, and visualized by autoradiography. The bands of C-terminal fragment (CTF) and N-terminal fragment (NTF) were predicted by Western blotting of S2 cell lysate co-expressing DmHtrA2 and FLAG-tagged DIAP1 (data not shown). (B) S2 cells were transfected with expression constructs for the indicated proteins and subjected to Cell Death assay. (C) DmHtrA2 was overexpressed in developing *Drosophila* eye using the GMR-GAL4 driver. The eyes at late pupal stage of wild-type, GMR-GAL4/UAS-DmHtrA2$^{2\ 6}$; *TM3, Sb*/+, and GMR-GAL4/UAS-DmHtrA2$^{2\ 6}$; UAS-p35/+ are shown.

chondria to extramitochondrial compartment, which in turn promotes cell death through inactivation of DIAP1. Indeed, a significant proportion of the *Drosophila* caspase DRONC, a fly counterpart of caspase-9, has been shown to localize near mitochondria [17]. Intriguingly, overexpression of DmHtrA2 caused caspase-independent cell death both *in vitro* and *in vivo*. This is consistent with the previous report that down-regulation of DIAP1 triggers a caspase activity-independent cell death pathway that is mediated by DRONC [18]. Our findings suggest that the mitochondrial regulation of cell death machinery could be conserved in *Drosophila*, and that the diverse roles of mitochondria in mammalian systems may have been coopted through the evolution of cell death mechanisms.

Acknowledgments

We thank Nanami Senoo-Matsuda, Hiroshi Kanda, and Ryoko Akai for technical support, Bloomington Stock Center for fly stocks, Yasushi Hiromi for the pWAGAL4 plasmid, Christine Hawkins for p49 plasmid, and John Gurdon and Ryusuke Niwa for the pUAS-GFP plasmid. This work was supported in part by grants from the Japanese Ministry of Education, Science, Sports, Culture and Technology (M.M. and R.T.), and was supported in part by RIKEN Bioarchitect Research Grant (M.M.). T.I. was supported by the Japan Society for the Promotion of Science, in part by a fellowship of Yamanouchi Foundation for Research on Metabolic Disorders, and is a recipient of the long-term fellowship from the Human Frontier Science Program. Y.S. was supported by the Special Postdoctoral Researchers Program, RIKEN.

Appendix A. Supplementary data

Supplementary data associated with this article can be found, in the online version, at doi:10.1016/j.bbrc.2007.03.079.

References

[1] X. Wang, The expanding role of mitochondria in apoptosis, Genes. Dev. 15 (2001) 2922–2933.

[2] D.D. Newmeyer, S. Ferguson-Miller, Mitochondria: releasing power for life and unleashing the machineries of death, Cell 112 (2003) 481–490.

[3] X. Saelens, N. Festjens, L. Vande Walle, M. van Gurp, G. van Loo, P. Vandenabeele, Toxic proteins released from mitochondria in cell death, Oncogene 23 (2004) 2861–2874.

[4] R. Hegde, S.M. Srinivasula, Z. Zhang, R. Wassell, R. Mukattash, L. Cilenti, G. DuBois, Y. Lazebnik, A.S. Zervos, T. Fernandes-Alnemri, E.S. Alnemri, Identification of Omi/HtrA2 as a mitochondrial apoptotic serine protease that disrupts inhibitor of apoptosis protein-caspase interaction, J. Biol. Chem. 277 (2002) 432–438.

[5] L.M. Martins, I. Iaccarino, T. Tenev, S. Gschmeissner, N.F. Totty, N.R. Lemoine, J. Savopoulos, C.W. Gray, C.L. Creasy, C. Dingwall, J. Downward, The serine protease Omi/HtrA2 regulates apoptosis by binding XIAP through a reaper-like motif, J. Biol. Chem. 277 (2002) 439–444.

[6] Y. Suzuki, Y. Imai, H. Nakayama, K. Takahashi, K. Takio, R. Takahashi, A serine protease, HtrA2, is released from the mitochondria and interacts with XIAP, inducing cell death, Mol. Cell. 8 (2001) 613–621.

[7] A.M. Verhagen, J. Silke, P.G. Ekert, M. Pakusch, H. Kaufmann, L.M. Connolly, C.L. Day, A. Tikoo, R. Burke, C. Wrobel, R.L. Moritz, R.J. Simpson, D.L. Vaux, HtrA2 promotes cell death through its serine protease activity and its ability to antagonize inhibitor of apoptosis proteins, J. Biol. Chem. 277 (2002) 445–454.

[8] J.M. Jones, P. Datta, S.M. Srinivasula, W. Ji, S. Gupta, Z. Zhang, E. Davies, G. Hajnoczky, T.L. Saunders, M.L. Van Keuren, T. Fernandes-Alnemri, M.H. Meisler, E.S. Alnemri, Loss of Omi mitochondrial protease activity causes the neuromuscular disorder of mnd2 mutant mice, Nature 425 (2003) 721–727.

[9] L.M. Martins, A. Morrison, K. Klupsch, V. Fedele, N. Moisoi, P. Teismann, A. Abuin, E. Grau, M. Geppert, G.P. Livi, C.L. Creasy, A. Martin, I. Hargreaves, S.J. Heales, H. Okada, S. Brandner, J.B. Schulz, T. Mak, J. Downward, Neuroprotective role of the Reaper-related serine protease HtrA2/Omi revealed by targeted deletion in mice, Mol. Cell. Biol. 24 (2004) 9848–9862.

[10] L.M. Martins, The serine protease Omi/HtrA2: a second mammalian protein with a Reaper-like function, Cell. Death. Differ. 9 (2002) 699–701.

[11] B.A. Hay, J.R. Huh, M. Guo, The genetics of cell death: approaches, insights and opportunities in Drosophila, Nat. Rev. Genet. 5 (2004) 911–922.

[12] T. Igaki, H. Kanuka, N. Inohara, K. Sawamoto, G. Nunez, H. Okano, M. Miura, Drob-1, a Drosophila member of the Bcl-2/CED-9 family that promotes cell death, Proc. Natl. Acad. Sci. USA 97 (2000) 662–667.

[13] L. Quinn, M. Coombe, K. Mills, T. Daish, P. Colussi, S. Kumar, H. Richardson, Buffy, a Drosophila Bcl-2 protein, has anti-apoptotic and cell cycle inhibitory functions, EMBO J. 22 (2003) 3568–3579.

[14] T. Igaki, M. Miura, Role of Bcl-2 family members in invertebrates, Biochim. Biophys. Acta 1644 (2004) 73–81.

[15] Y.J. Lin, L. Seroude, S. Benzer, Extended life-span and stress resistance in the Drosophila mutant methuselah, Science 282 (1998) 943–946.

[16] K.C. Zimmermann, J.E. Ricci, N.M. Droin, D.R. Green, The role of ARK in stress-induced apoptosis in Drosophila cells, J. Cell. Biol. 156 (2002) 1077–1087.

[17] L. Dorstyn, S. Read, D. Cakouros, J.R. Huh, B.A. Hay, S. Kumar, The role of cytochrome *c* in caspase activation in Drosophila melanogaster cells, J. Cell. Biol. 156 (2002) 1089–1098.

[18] T. Igaki, Y. Yamamoto-Goto, N. Tokushige, H. Kanda, M. Miura, Down-regulation of DIAP1 triggers a novel Drosophila cell death pathway mediated by Dark and DRONC, J. Biol. Chem. 277 (2002) 23103–23106.

Cell

Rac-GAP α-Chimerin Regulates Motor-Circuit Formation as a Key Mediator of EphrinB3/EphA4 Forward Signaling

Takuji Iwasato,[1,*] Hironori Katoh,[2] Hiroshi Nishimaru,[3] Yukio Ishikawa,[2] Haruhisa Inoue,[4] Yoshikazu M. Saito,[1] Reiko Ando,[1] Mizuho Iwama,[1] Ryosuke Takahashi,[4] Manabu Negishi,[2] and Shigeyoshi Itohara[1]

[1]Laboratory for Behavioral Genetics, RIKEN Brain Science Institute (BSI), 2-1 Hirosawa Wako-shi, Saitama 351-0198, Japan

[2]Laboratory of Molecular Neurobiology, Graduate School of Biostudies, Kyoto University, Yoshidakonoe-cho, Sakyo-ku, Kyoto 606-8501, Japan

[3]Neuroscience Research Institute, National Institute of Advanced Industrial Science and Technology (AIST), 1-1-1 Higashi, Tsukuba, Ibaraki 305-8566, Japan

[4]Department of Neurology, Kyoto University Graduate School of Medicine, 54 Kawahara-cho, Shogoin, Sakyo-ku, Kyoto 606-8507, Japan

*Correspondence: iwasato@brain.riken.jp

DOI 10.1016/j.cell.2007.07.022

SUMMARY

The ephrin/Eph system plays a central role in neuronal circuit formation; however, its downstream effectors are poorly understood. Here we show that α-chimerin Rac GTPase-activating protein mediates ephrinB3/EphA4 forward signaling. We discovered a spontaneous mouse mutation, *miffy* (*mfy*), which results in a rabbit-like hopping gait, impaired corticospinal axon guidance, and abnormal spinal central pattern generators. Using positional cloning, transgene rescue, and gene targeting, we demonstrated that loss of α-chimerin leads to *mfy* phenotypes similar to those of *EphA4*$^{-/-}$ and *ephrinB3*$^{-/-}$ mice. α-chimerin interacts with EphA4 and, in response to ephrinB3/EphA4 signaling, inactivates Rac, which is a positive regulator of process outgrowth. Moreover, downregulation of α-chimerin suppresses ephrinB3-induced growth cone collapse in cultured neurons. Our findings indicate that ephrinB3/EphA4 signaling prevents growth cone extension in motor circuit formation via α-chimerin-induced inactivation of Rac. They also highlight the role of a Rho family GTPase-activating protein as a key mediator of ephrin/Eph signaling.

INTRODUCTION

Ephrins are cell-surface-bound ligands for Eph receptors, which comprise the largest family of receptor tyrosine kinases (Eph Nomenclature Committee, 1997). The ephrin/Eph interaction induces bidirectional signaling: ephrin → Eph forward and Eph → ephrin reverse (Noren and Pasquale, 2004; Palmer and Klein, 2003). Ephrin/Eph signaling, which functions in short-range cell-to-cell communication primarily through repulsive effects, is central to neuronal circuit development (Flanagan and Vanderhaeghen, 1998; Palmer and Klein, 2003; Pasquale, 2005).

Downstream signaling has been studied mostly through in vitro cell culture experiments. Particularly important players in both forward and reverse signaling are the Rho-family GTPases (Rho-GTPases), such as RhoA, Rac, and Cdc42, which are the key regulators of actin dynamics (Etienne-Manneville and Hall, 2002; Luo, 2000; Noren and Pasquale, 2004; Wahl et al., 2000). Rho-GTPases are directly activated by Rho-guanine nucleotide-exchange factors (Rho-GEFs) and are inactivated by Rho-GTPase-activating proteins (Rho-GAPs). Accumulating evidence suggests that ephrin/Eph regulates Rho-GTPases through Rho-GEFs (Cowan et al., 2005; Irie and Yamaguchi, 2002; Murai and Pasquale, 2005; Ogita et al., 2003; Penzes et al., 2003; Shamah et al., 2001; Tanaka et al., 2004).

Among the numerous Rho-GEFs involved in ephrin/Eph signaling, ephexin1 is the best characterized. EphA receptors are thought to regulate growth cone dynamics through ephexin1 in axon guidance (Sahin et al., 2005; Shamah et al., 2001). Activation of RhoA induces growth cone retraction and/or collapse, while activated Rac and Cdc42 promote its extension (Etienne-Manneville and Hall, 2002; Luo, 2000). The engagement of Ephs by ephrin leads to activation of the GEF activity of ephexin1 toward RhoA, thereby causing growth cone collapse in vitro (Shamah et al., 2001). However, as *ephexin1*-knockout (KO) mice are apparently normal (Sahin et al., 2005), the role of ephexin1 remains largely unknown. It is also noteworthy that, compared with the considerable attention given to Rho-GEFs, the possible contribution of Rho-GAPs in actin dynamics controlled by ephrin/Eph signaling has largely been neglected.

The roles of ephrin/Eph signaling in vivo have been studied using mouse reverse genetics. An extremely well-characterized case is ephrinB3 → EphA4 forward signaling. *EphrinB3*$^{-/-}$ and *EphA4*$^{-/-}$ mice both display several neural phenotypes, including a rabbit-like hopping gait and impairment of two major motor circuits: the corticospinal tract (CST) and the spinal neuronal circuit controlling locomotion, which is also known as the central pattern generator (CPG). Similar phenotypes are also displayed by *EphA4*$^{KD/KD}$ and *EphA4*$^{FF/FF}$ mice, both of which have impaired kinase activity of EphA4, but not by mice expressing a truncated form of ephrinB3 lacking its cytoplasmic domain (Dottori et al., 1998; Kullander et al., 2003, 2001a, 2001b; Yokoyama et al., 2001). Thus, it is apparent that ephrinB3 → EphA4 forward signaling, but not EphA4 → ephrinB3 reverse signaling, is essential for the formation of these motor circuits.

CST axons controlling voluntary movements arise in the motor cortex, cross into the contralateral side of the medulla, and enter the spinal cord (Gianino et al., 1999; Liang et al., 1991). In wild-type (WT) mice, they rarely cross back to the other side in the spinal cord because ephrinB3 is anchored at the midline and generates repulsive signals through EphA4 receptors expressed on the surface of the CST axon membranes. In *ephrinB3* or *EphA4* mutant mice, due to a lack of repulsive ephrinB3/EphA4 forward signaling, many CST axons fail to stop at the midline and recross it (Kullander et al., 2001a; Yokoyama et al., 2001). Spinal CPGs are thought to generate the repetitive sequential stepping of limbs during walking (Grillner and Wallen, 1985). Locomotor-like rhythmic activity, alternating between the left and right sides, can be evoked in the isolated spinal cords of WT mice (Nishimaru and Kudo, 2000), whereas the activity of the two sides is synchronous in the spinal cords of *ephrinB3*$^{-/-}$ or *EphA4*$^{-/-}$ mice (Kullander et al., 2003). Aberrant midline crossing of axons from EphA4-expressing CPG interneurons is thought to be responsible for the CPG abnormality in *ephrinB3*$^{-/-}$ and *EphA4*$^{-/-}$ mice (Kiehn and Kullander, 2004; Kullander et al., 2003).

The current study provides both in vivo and in vitro evidence that the Rac-specific GAP α-chimerin plays a critical role in the formation of CST and CPGs as an essential downstream component of ephrinB3/EphA4 forward signaling.

RESULTS

A Novel Spontaneous Autosomal Recessive Mutation leading to a Rabbit-like Hopping Gait

We unexpectedly discovered mutant mice with a rabbit-like gait while generating mice homozygous for a ChAT-Cre#23 construct (Inoue et al., 2003). This mutation, which we designated as *miffy* (*mfy*), was autosomal recessive. We initially assumed that *mfy* was caused by gene disruption during transgene integration. However, this was not the case because the *mfy* locus segregated from the transgene, suggesting that the mutation arose spontaneously. *mfy/mfy* mice appeared in crosses at the expected Mendelian frequency and were healthy and fertile. Their bodies were slightly smaller than their littermate controls during the postnatal developmental period. For instance, on postnatal day 10 (P10), the average body weights ± standard error of the mean (SEM) were 4.68 ± 0.17 g, 5.68 ± 0.17 g, and 5.80 ± 0.15 g for the *mfy/mfy* (n = 10), *mfy/+* (n = 12), and +/+ (n = 5) pups, respectively. However, these differences were not evident in adulthood.

WT and *mfy/+* mice moved with a normal alternate step gait. By contrast, all of the *mfy/mfy* mice (n > 100) tended to move their left and right hind limbs synchronously, resulting in a rabbit-like hopping gait (Figure 1A). The mean ± SEM proportion of left-right synchronized gaits among 40 randomly selected gaits was 0 for *mfy/+* (n = 13) and 98.42% ± 0.61% for *mfy/mfy* (n = 19) mice ($p < 0.0001$, unpaired t test). The gross morphology of the *mfy/mfy* mouse brain was indistinguishable from that of its littermate controls (WT and *mfy/+* mice; Figures S1A and S1B). By contrast, a morphological analysis of cross-sections of the spinal cord of *mfy/mfy* mice revealed that the white matter in the dorsal funiculus was reduced, most prominently at the lumbar levels (Figure S1C).

Aberrant Recrossing of CST Axons at the Midline of the Spinal Cord in *mfy/mfy* Mice

The CST axons control voluntary movements through direct or indirect contact with spinal motor neurons (Liang et al., 1991). To visualize these axons, we injected anterograde tracer into the left motor cortex and stained the projections of the CST axons in the medulla and spinal cord. CST axons arising in the left motor cortex crossed to the right side of the medulla in both *mfy/mfy* and control mice (Figure S1D). However, in the spinal cord of control mice (n = 11), CST axons projected only into the contralateral (right) gray matter and barely recrossed the midline into the ipsilateral gray matter, whereas we observed aberrant midline recrossing of these axons in all of the preparations of *mfy/mfy* mouse spinal cords examined (n = 7; Figures 1B and 1C).

To confirm the anterograde tracing results, we injected a retrograde tracer unilaterally into the lumber spinal cord (Figure 1D). In WT mice, most of the retrograde-labeled CST neurons were located in layer V of the contralateral motor cortex (Figure 1E). However, in *mfy/mfy* mice, the ipsilateral cortex also contained many labeled neurons (Figure 1F). Cell-count analyses of the motor cortex revealed that the ipsilateral cortex of WT (n = 4) and *mfy/mfy* (n = 7) mice contained 2.02% ± 0.92% and 34.26% ± 5.22% times as many labeled cells as the contralateral cortex, respectively, which was statistically significant ($p < 0.002$; Figure 1G).

Abnormal CPGs in the Spinal Cord of *mfy/mfy* Mice

To examine the locomotor CPGs underlying limb movements during walking, we isolated the spinal cords from newborn (P1–P3) *mfy/mfy* and control (*mfy/+* and WT) mice and induced locomotor-like activity by applying

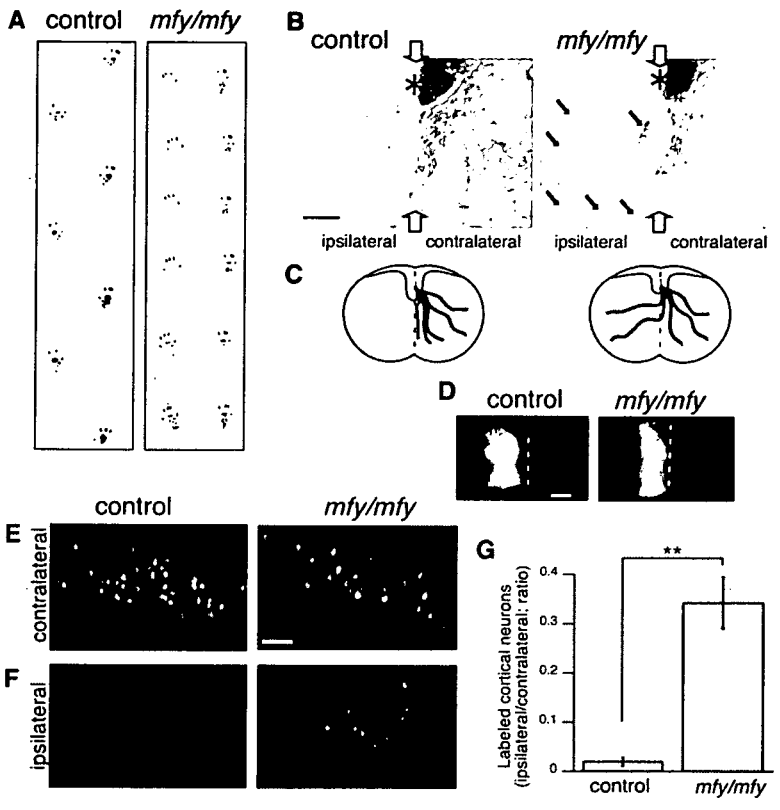

Figure 1. Abnormal Walking and CST Axon Guidance in the Novel Spontaneous Mutant *mfy*

(A) Representative hind-limb footprint patterns. Hind limbs were painted with black ink, and the mice were placed on white paper.

(B) Anterograde tracings of CST axons by biotinylated dextran amine (BDA) and sectioning at cervical levels of the spinal cord. CST axons positioned within the dorsal funiculus (asterisk) on the contralateral side to the tracer injection projected into the spinal gray matter in both control and *mfy/mfy* mice; however, in the *mfy/mfy* mice only, many of the CST axons (blue arrows) recrossed the midline (white arrows).

(C) Schematics of CST axons (red) in the spinal cord.

(D) A fluorescent retrograde tracer cholera toxin B (CTB) was unilaterally injected into the lumbar spinal cord.

(E and F) In the motor cortex layer V of control (WT) mice, most of the labeled neurons were located in the contralateral side (E). In *mfy/mfy* mice, the ipsilateral side also contained many labeled neurons (F).

(G) The ipsilateral/contralateral ratio of numbers of labeled cortical neurons in *mfy/mfy* mice (n = 7) was significantly higher than that of control mice (n = 4). Data are represented as the mean ± SEM: Student's t test, $p < 0.002$. Scale bars: 100 μm.

N-methyl-D-aspartate (NMDA) and serotonin. The ventral root (VR) activity of lumber 2 (L2) represents flexor muscle activity during locomotion, while that of L5 represents extensor activity (Whelan et al., 2000). In control mice, we observed alternation between the left and right L2s (Figures 2A–2C), whereas the cords of *mfy/mfy* mice displayed a synchronous rhythm of the left and right L2s (Figures 2A–2C). The rhythmic activity of the flexors (L2) and extensors (L5) of each limb alternated in both control and *mfy/mfy* mice spinal cords (Figures 2A–2C). We injected a tracer unilaterally into the ventral side of the spinal cords of P4 *mfy/mfy* and control pups, and we found that more neuronal fibers, presumably derived from ipsilateral-projecting interneurons, crossed the midline in the *mfy/mfy* spinal cords than in the control spinal cords (Figure 2D; for quantitative analyses, see Figures S2A and S2B).

The *mfy* Locus Encodes the Rac-Specific GAP α-Chimerin

To locate the *mfy* locus, we employed microsatellites and single-nucleotide polymorphisms (SNPs) that distinguish between the alleles of two inbred mouse strains, DBA/2 (DBA) and C57BL/6 (B6). The *mfy* mutant was identified and maintained in a pure B6 genetic background. We therefore crossed *mfy/mfy* mice with WT DBA mice and obtained *mfy/+* mice in a B6/DBA F_1 genetic background. By backcrossing these F_1 mice to *mfy/mfy* mice and genotyping the DNA of the 299 backcross progeny, we mapped the *mfy* locus to the region between SNPs *rs13476571* and *rs13459064* on chromosome 2 (Figure S3).

In total, 30 genes are known within this 3.27 Mb interval (Table S1). Among these, 10 genes could be excluded because their KO mouse lines have been previously reported to survive to adulthood, and they do not appear to have hopping gaits (for references, see Table S1). We compared the sizes and transcript levels of the remaining 20 genes in the brains of WT and *mfy/mfy* mice at P5 using the reverse transcription-polymerase chain reaction (RT-PCR) with primer sets amplifying the complementary DNA (cDNA) between the 5′ and 3′ untranslated regions (UTRs) and found that the transcripts of only one gene, the α-chimerin (*α-Chn*) gene, differed in size (Figures 3A and 3B; Table S1). α-chimerin is a Rho-GAP that is specific for the positive regulator of actin polymerization, Rac (Diekmann et al., 1991; Hall et al., 1990, 1993). Recent reports using overexpression and/or small-interfering RNA (siRNA)-mediated knockdown in cultured neurons and/or tissue slices suggest that α-chimerin is involved in regulating dendritic morphology and spine density (Buttery et al., 2006; Van de Ven et al., 2005) as well as semaphorin3A-induced growth cone collapse (Brown et al., 2004). However, the role of α-chimerin in living animals has not yet been defined.

α-Chn has two splice isoforms: α1 and α2 (Hall et al., 1990, 1993). A comparison of the sequences of the *α1-Chn* and *α2-Chn* cDNAs of WT and *mfy/mfy* mice revealed that exon 9 (174 base pairs [bp]) was deleted in the

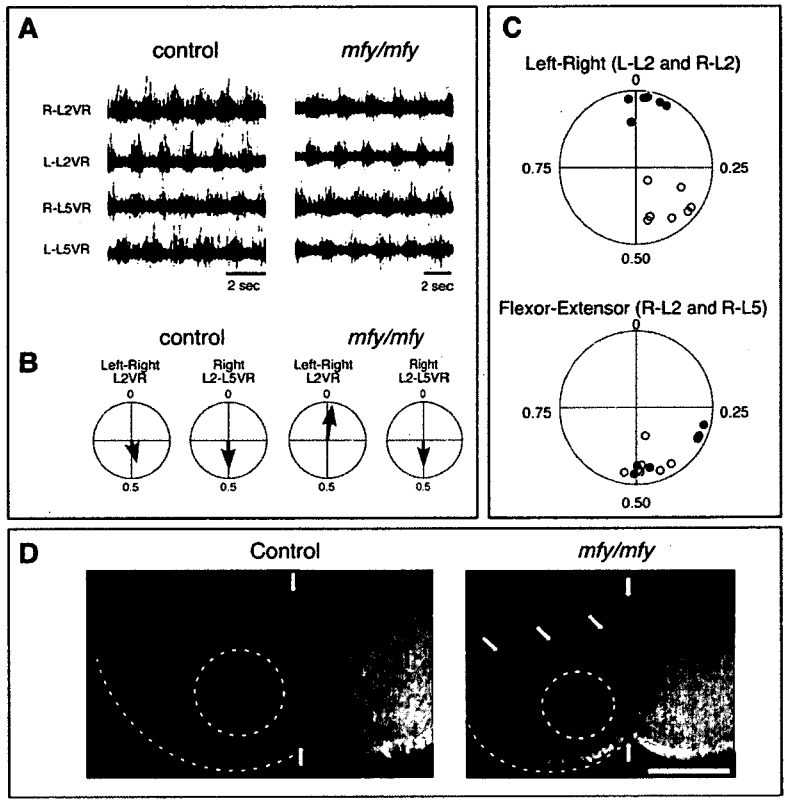

Figure 2. Synchronous Left-Right VR Activity in the Lumbar Spinal Cord of *mfy/mfy* Mice

(A) Locomotor-like motor activity recorded after bath-application of NMDA and serotonin to isolated spinal cords of control and *mfy/mfy* mice. VR activity of the second (L2) and fifth (L5) lumbar segments on the left (L-) and right (R-) sides was recorded using glass-suction electrodes.

(B) Circular phase diagrams for the locomotor-like rhythmic activity of the control and *mfy/mfy* mice shown in (A). Phase relationships between L-L2VR and R-L2VR (left panel) and flexor (R-L2VR) and extensor (R-L5VR) on one side of the lumbar cord (right panel) are indicated in each diagram derived from 30 locomotor cycles. Locomotor cycles in which the two VR activities are in complete alternation have phase values of 0.5. Those that are completely synchronous have phase values of 0 or 1. The mean phase and the *r* value, which describes the concentration of phase values around the mean, are shown by the direction and magnitude, respectively, of the vector originating from the center of the circle.

(C) Summary plots of seven control (open circles) and six *mfy/mfy* (filled circles) mice at P1–P3.

(D) Transverse spinal cord sections (100 μm thick) at the L2 level after unilateral application of DiI on the ventral side of L4. More neuronal fibers (yellow arrows), which are likely to be derived from ipsilateral-projecting interneurons, crossed the midline (white arrows) to the contralateral (left) side in *mfy/mfy* spinal cords than in control spinal cords. The cell bodies of descending commissural interneurons, shown by dotted circles, were indistinguishable. Scale bar: 500 μm.

α*1-Chn*^{mfy} and α*2-Chn*^{mfy} transcripts (Figure 3A). Exon 9 encodes 58 amino acids, three of which (EIE) are known to be essential for the GAP activity of α-chimerin that inactivates Rac (Ahmed et al., 1994); α2-chimerin^{mfy} was indeed found to lack Rac-GAP activity in vitro (Figure S4). In addition to the α1 and α2 isoforms, we found transcripts of a putative novel isoform that we termed α3 (Figures 3A and 3B). In the α*3-Chn*^{mfy} transcript, four nucleotides (GATG) of exon 9, including the putative initiation codon, were replaced with retroposon sequences, and intron 9 failed to be excised (Figure 3A). The cloning and sequencing of the genomic DNA of the *mfy* allele revealed an insertion of a retroposon into exon 9, which appeared to impair both the donor and the acceptor splicing functions (Figure 3A). Quantitative RT-PCR demonstrated strong α*2-Chn* expression, weak α*1-Chn* expression, and little α*3-Chn* expression in the motor cortex and spinal cord of P4 WT mice (Figure 3C). We therefore focused on the α2 isoform in subsequent studies. We raised an α2-chimerin-specific polyclonal antibody and confirmed by western blot analysis that the α2-chimerin^{WT} protein could not be detected in the *mfy/mfy* brain (Figure 3D). Furthermore, even the α2-chimerin^{mfy} protein was barely detected in the *mfy/mfy* brain and spinal cord (Figures 3D and 3E), suggesting that endogenous α2-chimerin^{mfy} is much less stable in neurons than α2-chimerin^{mfy} overexpressed in cultured cells (Figure S4B).

Improved Locomotor Behavior of *mfy/mfy* Mice Expressing Transgenic α-*Chn*

To confirm that α-*Chn* was the *mfy* gene, we tested whether transgenic (Tg) expression of α-*Chn* rescued the *mfy* phenotype. We modified a bacterial artificial chromosome (BAC) clone that covered the 49 kb upstream region and exons 1–7 of α-*Chn* using Red/ET homologous recombination and flp/FRT recombination in order to make a BAC α-*Chn* construct in which exon 7 was followed by a cDNA encoding exons 8–13 and a poly(A) signal (Figure 4A). We then generated two lines (#539 and #883) of BAC Tg mice by microinjecting the construct into pronuclei and mated them with *mfy/mfy* mice to obtain Tg mice in the *mfy/mfy* background (Figure 4B). There were no improvements in the gaits of the Tg#539:*mfy/mfy* mice (see Figure S5 legend), consistent with no detectable

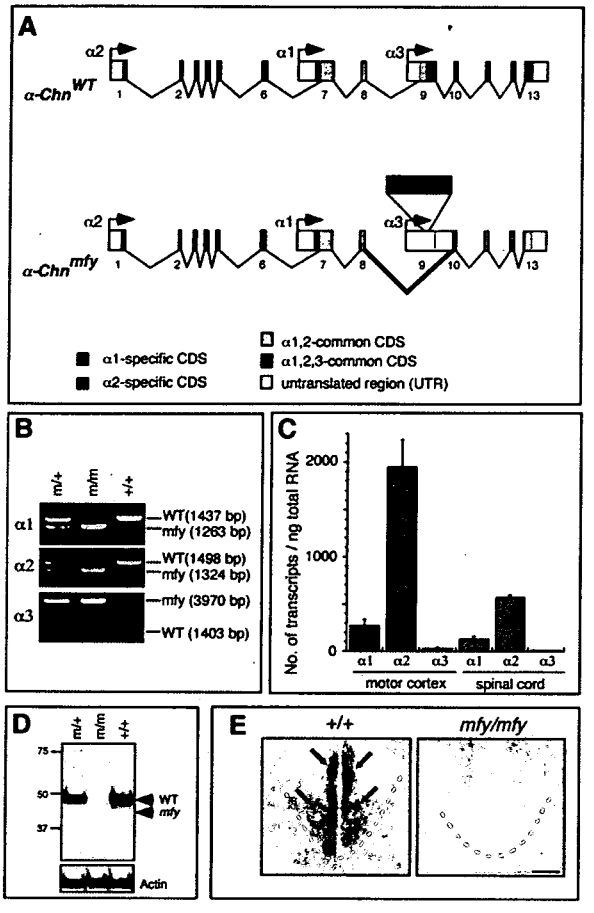

Figure 3. The *mfy* Locus Encodes α-Chimerin Rac-GAP

(A) Schematic exon-intron structures of *α1-Chn*, *α2-Chn*, and *α3-Chn* splicing variants for the WT (*α-Chn*^{WT}) and *mfy* (*α-Chn*^{mfy}) alleles. Retroposon (Tn) insertion into exon 9 in the *mfy* mutant resulted in deletion (red lines) of exon 9 (174 bp) in the *α1* and *α2* transcripts, and deletion of four nucleotides (including the putative initiation codon) and failure of intron 9 splicing in the *α3* transcript. CDS: coding sequences.

(B) RT–PCR products from between the 5′ UTR and the 3′ UTR of the *α1-Chn*, *α2-Chn*, and *α3-Chn* splicing isoforms in cDNAs derived from WT (+/+), *mfy*/+ (m/+), and *mfy/mfy* (m/m) brains at P5. PCR products from the WT and mutant (mfy) *α1-Chn*, *α2-Chn*, and *α3-Chn* isoforms were purified and cloned, and their nucleotide sequences were determined.

(C) *α2-Chn* predominates in the developing motor cortex and spinal cord. Real-time quantitative RT-PCR of *α1-Chn*, *α2-Chn*, and *α3-Chn* in the motor cortex and spinal cord of WT mice at P4. All data are presented as the mean ± SEM (n = 3 mice).

(D) Western blot using an α2-chimerin-specific antibody revealed that α2-chimerin^{WT} protein (WT) was absent from *mfy/mfy* mice. Unexpectedly the mutant protein (mfy) was barely detectable in *mfy*/+ and *mfy/mfy* mice. Total lysates from P10 of the mouse telencephalon were used.

(E) Immunohistochemistry using α2-chimerin-specific antibody revealed strong expression of α2-chimerin in the CST (arrows) of the dorsal funiculus (dotted line) of the WT spinal cord, suggesting that α2-chimerin functions in developing CST axons. α-chimerin was not detectable in *mfy/mfy* spinal cords. Scale bar: 50 μm.

α-chimerin expression in these mice (Figures S5A and S5B). By contrast, considerable improvement was observed in the gaits of the Tg#883:*mfy/mfy* mice (Figure 4C). The average ± SEM proportion of left-right synchronized gaits in 40 randomly selected gaits of Tg#883:*mfy/mfy* mice (n = 13) was 53.65% ± 6.56%, which was substantially less than in their littermate *mfy/mfy* mice (n = 6, 99.58% ± 0.42%; $p < 0.0001$, unpaired t test). α-chimerin protein was expressed at low levels in Tg#883:*mfy/mfy* mice (Figures S5A–S5C), which was consistent with the moderate rescue of gait observed in these mice. These results strongly suggest that *α-Chn* is the causal gene of the *mfy* mutation.

Generation and Characterization of *α-Chn* KO Mice

To further confirm that the *mfy* gene encoded *α-Chn*, we deleted exons 9 and 10 from the allele by a gene-targeting technique in embryonic stem (ES) cells and Cre/loxP recombination in the mouse germline and generated mice homozygous for the targeted allele (*α-Chn* KO mice; Figures 4D and S5D). These mice had a hopping gait similar to that of *mfy/mfy* mice (Figure 4E). They also demonstrated aberrant midline recrossing of CST axons (Figure 4F), aberrant midline crossing of spinal local circuit neurons (Figure S2C), and shorter ventral extension of the dorsal funiculus in the spinal cord (data not shown). Furthermore, they showed abnormal spinal CPGs (Figures 4G and S6). All of these phenotypes were similar to those of *mfy/mfy* mice. Thus, we concluded that the *mfy* phenotypes were caused by *α-Chn* disruption.

Localization of α-Chimerin Proteins in CST

The phenotypes of *mfy/mfy* and *α-Chn* KO mice (hopping gait, Figures 1A and 4E), abnormal spinal-cord morphology (Figure S1C), abnormal CPGs (Figures 2C and 4G), aberrant midline crossing by CPG axons (Figures 2D and S2), and aberrant midline recrossing by CST axons (Figures 1B and 4F) appeared to be identical to those reported for *ephrinB3*$^{-/-}$ and *EphA4*$^{-/-}$ mice (Dottori et al., 1998; Kullander et al., 2003, 2001a; Yokoyama et al., 2001) and for *EphA4*$^{FF/FF}$ and *EphA4*$^{KD/KD}$ mice expressing a mutant EphA4 lacking kinase activity (Kullander et al., 2001b). Nevertheless, the anterior commissure, the formation of which is known to be dependent on EphA4 reverse signaling (Kullander et al., 2001b), appeared normal in *mfy/mfy* mice (Figure S1B). Hence, it seemed likely that the *mfy* phenotype was caused by impairment of ephrinB3/EphA4 forward signaling.

Using immunohistochemistry, we found that α2-chimerin colocalized with EphA4 in the developing CST (Figures S7A and S7C). In *α-Chn* KO CST, α2-chimerin was not detected, but the levels of EphA4 expression appeared to be unaltered (Figures S7B and S7D). We also found that the α2-chimerin protein was present in the growth cones of cultured neurons derived from the anterior dorsomedial to dorsal neocortex (motor cortex; Figure S8C). These results suggest that α-chimerin functions

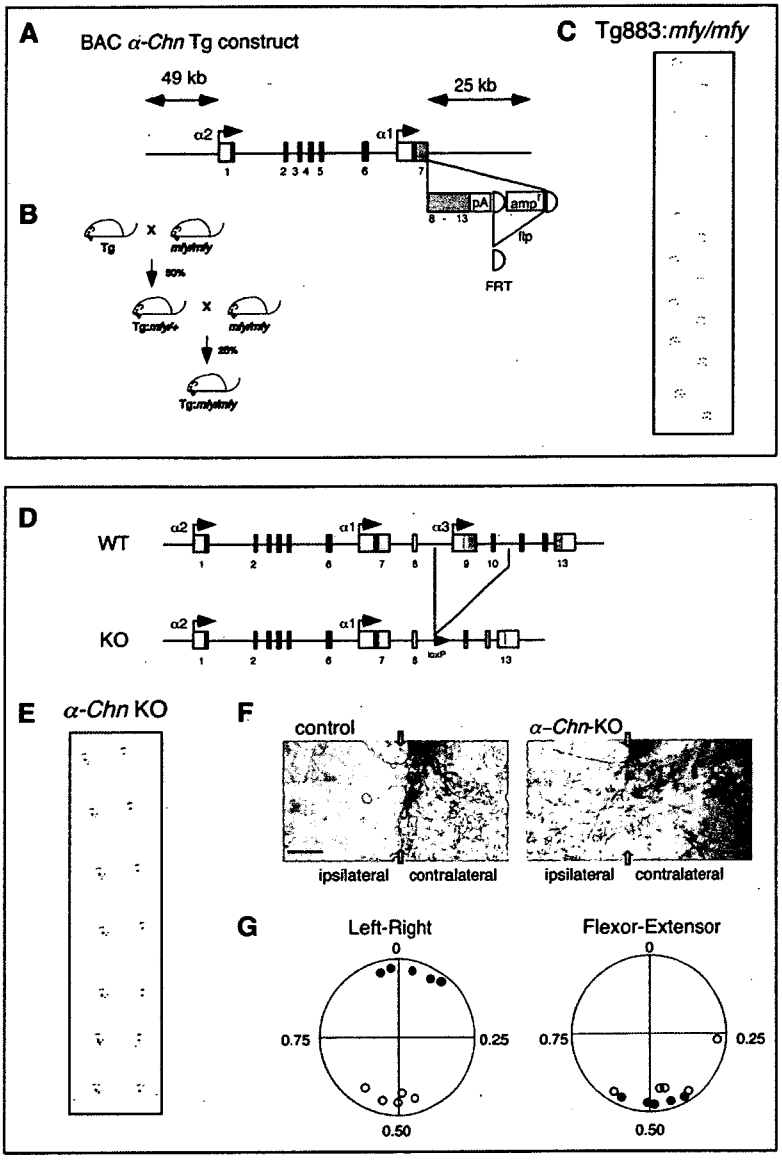

Figure 4. Disruption of α-*Chn* Is Responsible for the *mfy* Phenotypes

(A) Schematic of the BAC Tg construct. A cDNA fragment containing exons 8–13, a poly(A) signal, and an *amp*^{r} selection marker flanked by two FRT sites was inserted immediately after exon 7 of a BAC clone covering exons 1–7 of α-*Chn*, using Red/ET homologous recombination in bacteria. *Amp*^{r} was removed from the BAC construct by expressing flp recombinase in the bacterial clone.

(B) Tg mouse lines were generated by injecting the linearized construct into fertilized mouse eggs. Two lines of Tg mice were crossed with *mfy/mfy* mice to yield Tg:*mfy/+* mice. These were then crossed with *mfy/mfy* mice to obtain Tg mice in a *mfy/mfy* background.

(C) Improved walking of Tg#883:*mfy/mfy* mice. All Tg#883:*mfy/mfy* mice showed a marked improvement in the control of walking.

(D) Schematic of the KO allele, in which exons 9 and 10 were deleted by homologous recombination in ES cells, and Cre/loxP recombination in the mouse germline.

(E) Representative hind-limb footprint patterns of α-*Chn* KO mice showing a hopping gait similar to that of *mfy/mfy* mice.

(F) Anterograde tracing of CST axons and sectioning at cervical levels of the spinal cord. CST axons of α-*Chn* KO mice aberrantly recrossed the spinal cord midline, as seen in *mfy/mfy* mice. Scale bar: 100 μm.

(G) Circular phase diagrams for the locomotor-like activity of five control (open circles) and five α-*Chn* KO (filled circles) mice at P1–P3. Left-right VR activity in the lumber spinal cord of α-*Chn* KO mice was synchronous as that of *mfy/mfy* mice.

as a downstream mediator of ephrinB3/EphA4 forward signaling in developing CST axons.

Interaction between α-Chimerin and EphA4

To test whether α-chimerin interacts with EphA4, we co-transfected 293T cells with *EphA4* and α-*Chn*-expression constructs and immunoprecipitated EphA4 from cell lysates with Fc region-fused ephrinA1. Both α1-chimerin and α2-chimerin were precipitated with EphA4^{WT} and kinase-dead EphA4^{FF} (Figure 5A), and α2-chimerin^{mfy} was also precipitated with EphA4 (Figure S9). These results suggest that α-chimerin interacts with EphA4 in vitro and that this interaction does not require the kinase activity of EphA4 or the GAP activity of α-chimerin. To identify the region of α-chimerin responsible for interacting with EphA4, we performed an in vitro glutathione S-transferase (GST) fusion protein pull-down assay. EphA4 was co-precipitated with full-length α2-chimerin and the α1- and α2-common carboxy (C) terminus, but not with the α2-specific amino (N)-terminus (Figure 5B). These results show that EphA4 associates with α1-chimerin and α2-chimerin at their C termini.

Next we examined whether α-chimerin interacts with EphA4 in neurons, and, if so, whether ligand stimulation enhances the interaction. EphA4 was coprecipitated with α2-chimerin without ligand stimulation, and the amount of EphA4 precipitated with α2-chimerin was not increased following stimulation with clustered ephrinB3 (Figure 5C). These results indicate that α-chimerin associates with EphA4 in neurons and that this interaction is independent of ephrinB3-stimulation. Finally, we prepared lysates from the developing motor cortex of WT mice and immunoprecipitated them with anti-α2-chimerin antibody. EphA4 was again precipitated with α2-chimerin (Figure 5D).

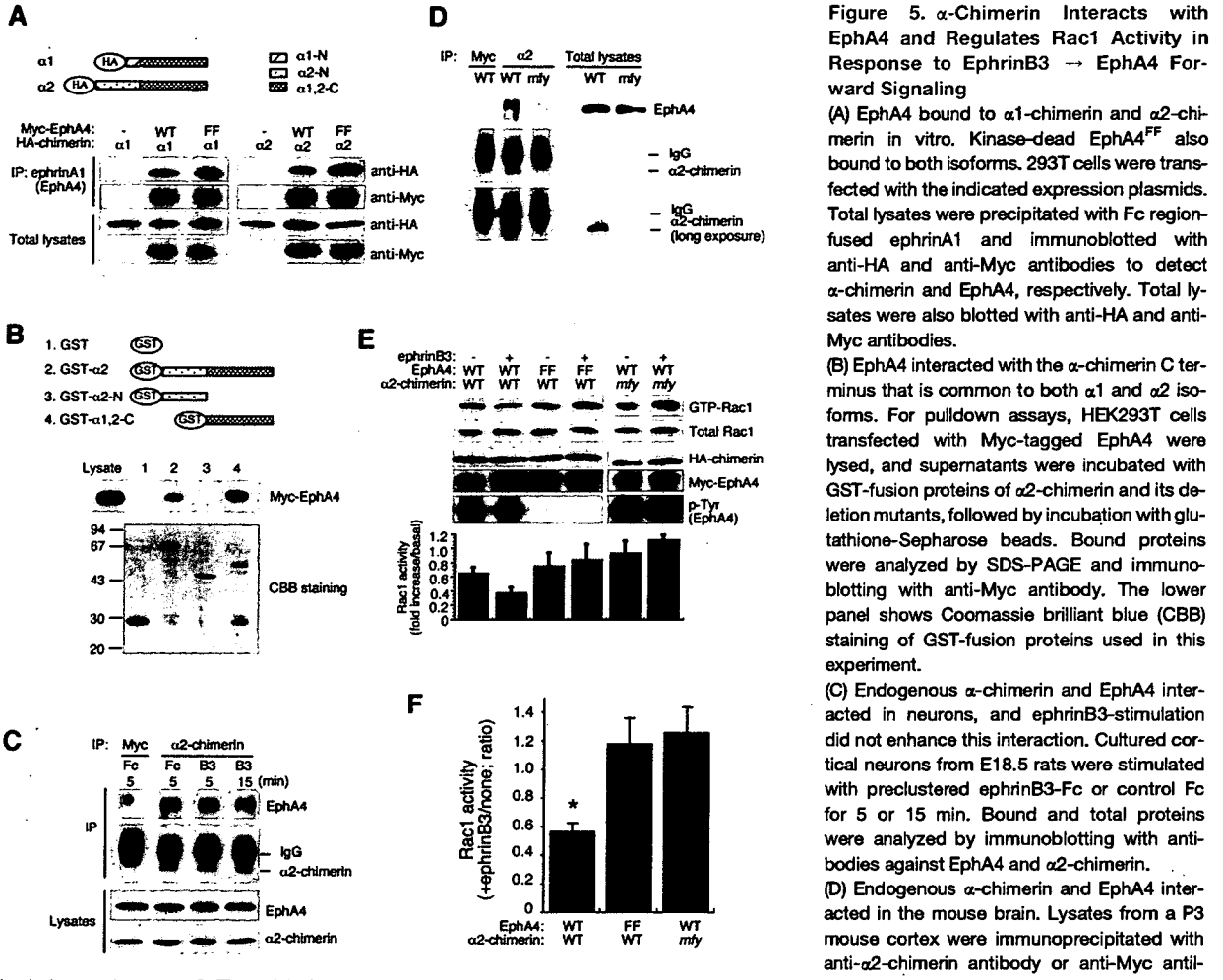

Figure 5. α-Chimerin Interacts with EphA4 and Regulates Rac1 Activity in Response to EphrinB3 → EphA4 Forward Signaling

(A) EphA4 bound to α1-chimerin and α2-chimerin in vitro. Kinase-dead EphA4^{FF} also bound to both isoforms. 293T cells were transfected with the indicated expression plasmids. Total lysates were precipitated with Fc region-fused ephrinA1 and immunoblotted with anti-HA and anti-Myc antibodies to detect α-chimerin and EphA4, respectively. Total lysates were also blotted with anti-HA and anti-Myc antibodies.

(B) EphA4 interacted with the α-chimerin C terminus that is common to both α1 and α2 isoforms. For pulldown assays, HEK293T cells transfected with Myc-tagged EphA4 were lysed, and supernatants were incubated with GST-fusion proteins of α2-chimerin and its deletion mutants, followed by incubation with glutathione-Sepharose beads. Bound proteins were analyzed by SDS-PAGE and immunoblotting with anti-Myc antibody. The lower panel shows Coomassie brilliant blue (CBB) staining of GST-fusion proteins used in this experiment.

(C) Endogenous α-chimerin and EphA4 interacted in neurons, and ephrinB3-stimulation did not enhance this interaction. Cultured cortical neurons from E18.5 rats were stimulated with preclustered ephrinB3-Fc or control Fc for 5 or 15 min. Bound and total proteins were analyzed by immunoblotting with antibodies against EphA4 and α2-chimerin.

(D) Endogenous α-chimerin and EphA4 interacted in the mouse brain. Lysates from a P3 mouse cortex were immunoprecipitated with anti-α2-chimerin antibody or anti-Myc antibody (a negative control). The *mfy/mfy* cortex was used as a second negative control. Bound and total proteins were analyzed by immunoblotting with antibodies against EphA4 and α2-chimerin.

(E) COS-7 cells transfected with the indicated plasmids were stimulated with preclustered ephrinB3-Fc (+) or Fc (–) for 10 min. GTP-bound Rac1 was identified by SDS-PAGE and immunoblotting, and its levels were measured and normalized to the corresponding total Rac1 levels. The means and SEMs of Rac1 activity (fold increase/basal) are shown at the bottom.

(F) Statistical analysis of the data shown in (E). EphrinB3-stimulation inactivated Rac1 in cells expressing both EphA4^{WT} and α-chimerin^{WT}, but not in cells expressing EphA4^{FF} and α-chimerin^{WT} or EphA4^{WT} and α-chimerin^{mfy}. n = 4 (EphA4^{WT} + α2-chimerin^{WT}), 5 (EphA4^{FF} + α2-chimerin^{WT}), or 3 (EphA4^{WT} + α2-chimerin^{mfy}). All data are presented as the mean ± SEM. (*$p < 0.05$, ANOVA/Tukey HSD).

α-Chimerin Inactivates Rac in Response to EphrinB3/EphA4 Forward Signaling In Vitro

No previous reports have suggested the involvement of α-chimerin in ephrin/Eph signaling. To determine whether α-chimerin regulates Rac activity in response to ephrinB3/EphA4 forward signaling, we transfected COS-7 cells with EphA4 (EphA4^{WT} or kinase-dead EphA4^{FF}) and α2-chimerin (α-chimerin^{WT} or α-chimerin^{mfy}) and measured the Rac activity in the presence or absence of ephrinB3 stimulation (Figure 5E). We found that ephrinB3 stimulation inactivated Rac in cells expressing EphA4^{WT} and α-chimerin^{WT}, but not in cells expressing either EphA4^{FF} and α-chimerin^{WT} or EphA4^{WT} and α-chimerin^{mfy} (Figure 5F). These results indicate that both EphA4 kinase activity and functional α-chimerin are required for ephrinB3 stimulation to inactivate Rac. It is noteworthy that the EphA4 proteins overexpressed in COS cells were phosphorylated, and, therefore, kinase active, but were unable to fully activate α-chimerin in the absence of ephrinB3 stimulation (Figure 5E). These results suggest that EphA4 kinase activity alone is not sufficient for activating the Rac-GAP of α-chimerin (see Discussion).

Downregulation of α-Chimerin Suppresses EphrinB3-Induced Growth Cone Collapse in Cultured Cortical Neurons

EphrinB3/EphA4 forward signaling induces growth cone collapse in cultured neurons derived from the motor cortex (Egea et al., 2005; Kullander et al., 2001a). To determine whether α-chimerin regulates growth cone dynamics downstream of ephrinB3/EphA4 forward signaling, we performed two experiments. First, we cultured neurons

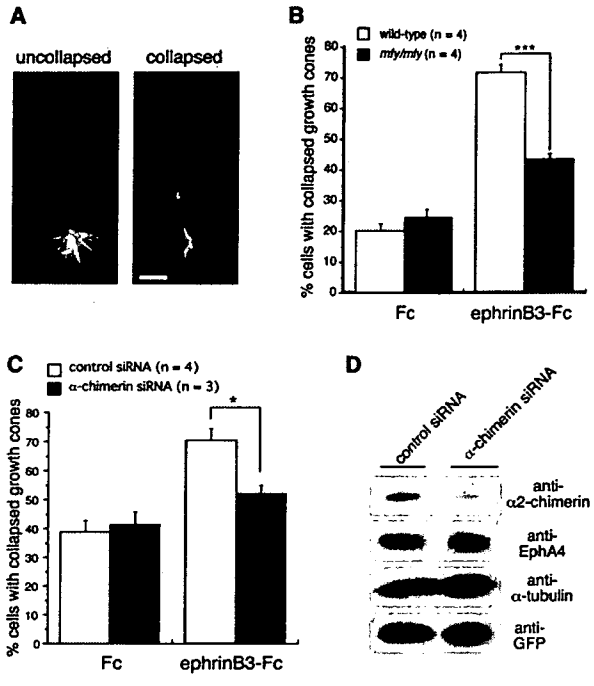

Figure 6. Downregulation of α-Chimerin Suppresses EphrinB3-Induced Growth Cone Collapse

(A) Representative examples of growth cones in phalloidin-stained cultured cortical neurons treated with preclustered Fc control (uncollapsed) or ephrinB3-Fc (collapsed). Scale bar: 10 μm.

(B) Growth cone collapse was induced by ephrinB3 in cultured neurons derived from the WT motor cortex, but was barely seen in those derived from the *mfy/mfy* cortex. All data are presented as the mean ± SEM of four independent experiments in each of which 100 neurons were counted (***$p < 0.001$, Student's t test).

(C) Downregulation of α-chimerin by siRNA suppressed ephrinB3-induced growth cone collapse in cultured cortical neurons. Cultured neurons derived from E18.5 rat cortex were transfected with a plasmid expressing both siRNA and enhanced yellow fluorescent protein (EYFP). In each experiment, 34–67 neurons expressing EYFP were counted. (*$p < 0.05$, Student's t test).

(D) α-chimerin-specific siRNA reduced the level of α-chimerin protein but not EphA4 protein. A 58.5% reduction of α-chimerin protein was observed in total lysates from cultured neurons in which 62% (not shown) of cells expressed α-chimerin-specific siRNA/EYFP, suggesting a drastic (>90%) reduction of α-chimerin.

derived from the motor cortex of WT and *mfy/mfy* mice on embryonic day 16.5 (E16.5) and then stimulated them with preclustered Fc or ephrinB3-Fc. EphrinB3 efficiently induced growth cone collapse in WT cortical neurons, as previously reported (Kullander et al., 2001a; Figures 6A and 6B); however, in the *mfy/mfy* cortical neurons, the frequency of collapse was significantly reduced (Figure 6B). Second, we expressed α-chimerin-specific siRNA by transfecting an expression vector into cultured neurons derived from the E18.5 rat motor cortex (Figure S8). The frequency of ephrinB3-induced growth cone collapse was significantly reduced in transected neurons (Figure 6C), and western blotting with the anti-α2-chimerin antibody demonstrated that α-chimerin protein levels were drastically reduced (>90%) in the transfected neurons (Figure 6D). We concluded that α-chimerin Rac-GAP acts downstream of ephrinB3/Eph signaling to cause growth cone collapse of cortical neurons.

Taken together, the results of our in vivo and in vitro studies confirm that α-chimerin Rac-GAP is a key molecule linking ephrinB3-induced EphA4 activation to the inactivation of Rac—a positive regulator of process outgrowth—thereby causing growth cone retraction and, eventually, axonal repulsion at the spinal cord midline.

DISCUSSION

α-Chimerin Is a Key Mediator of EphrinB3/EphA4 Forward Signaling and Causes Repulsion of CST Axons at the Spinal Cord Midline

We have shown the following. First, α-chimerin is colocalized with EphA4 in the developing CST (Figure S7). Second, it interacts with EphA4 both in vitro and in vivo (Figures 5A–5D). Third, when EphA4 is stimulated by ephrinB3, α-chimerin inactivates Rac, which is a positive regulator of process outgrowth, in vitro (Figure 5F). Fourth, ephrinB3-induced growth cone collapse is suppressed in cultured cortical neurons in which α-chimerin is downregulated by RNAi or *mfy* mutation (Figure 6). Fifth and finally, repulsion of CST axons at the spinal cord midline (Figures 1B and 4F) and formation of spinal CPGs (Figures 2C and 4G) are impaired in *mfy/mfy* mice and *α-Chn* KO mice, and both of these processes depend on ephrinB3/EphA4 forward signaling (Kullander et al., 2003, 2001a, 2001b; Yokoyama et al., 2001). Our results show that the Rac-GAP α-chimerin regulates CST axon guidance and CPG formation by mediating ephrinB3/EphA4 forward signaling (Figure 7).

It has been proposed that EphA receptors regulate growth cone dynamics through Rho-GEF ephexin1 (Shamah et al., 2001). During this process, activation of RhoA induces growth cone retraction and/or collapse, while activated Rac and Cdc42 promote its extension (Etienne-Manneville and Hall, 2002; Luo, 2000). The engagement of Ephs by ephrin leads to preferential activation of the exchange activity of ephexin toward RhoA, thus leading to growth cone collapse in vitro (Figure 7A; Shamah et al., 2001). We showed that the ephrin/Eph interaction leads to growth cone collapse due to Rac inactivation via the GAP activity of α-chimerin (Figure 7A). As both ephexin1 and α-chimerin are enriched in the central nervous system (Hall et al., 2001, 1993; Shamah et al., 2001), it is likely that the cooperative action of ephexin1-induced RhoA activation and α-chimerin-induced Rac inactivation function to induce retraction of growth cones during axon guidance in various circuits. *Ephexin1* KO mice appear to be normal (Sahin et al., 2005). This absence of an obvious phenotype might be due to compensation by other ephexin family members. Alternatively, it might be due to the activity of α-chimerin, which could prevent growth cone extension by inactivating Rac in response to ephrin/Eph signaling, even in the absence of